THESIS FOR THE DEGREE OF DOCTOR OF PHILOSOPHY IN SOLID AND STRUCTURAL MECHANICS

Model-Based Condition Monitoring of Railway Switches and Crossings

MARKO D.G. MILOŠEVIĆ

Department of Mechanics and Maritime Sciences

CHALMERS UNIVERSITY OF TECHNOLOGY

Gothenburg, Sweden 2024

Model-Based Condition Monitoring of Railway Switches and Crossings
MARKO D.G. MILOŠEVIĆ

Thesis for the degree of Doctor of Philosophy – Department of Mechanics and Maritime Sciences
ISBN: 978-91-8103-036-5
Serial number 5494 for PhD dissertations at Chalmers in ISSN 0346-718XDepartment of Mechanics and Maritime Sciences
Division of Dynamics
Chalmers University of Technology
SE-412 96 Gothenburg
Sweden
Telephone + 46 (0)31-772 1000

Cover: MBS model during a crossing transition in Simpack software

Chalmers Reproservice
Gothenburg, Sweden 2024

Model-Based Condition Monitoring of Railway Switches and Crossings
MARKO D.G. MILOŠEVIĆ
Department of Mechanics and Maritime Sciences
Chalmers University of Technology

Abstract

Railway switches and crossings, often known as S&C or turnouts, enable trains to change track. This operating feature comes at a cost because S&C have rail discontinuities which cause a significant contribution to the dynamic loading and higher degradation rates compared to ordinary plain line track. These higher rates of deterioration present a promising opportunity for implementing condition monitoring systems that have the potential to enhance maintenance decision-making and surpassing the capabilities of periodic inspections conducted by measurement cars or track engineers. This thesis is therefore focused on developing novel processing tools to increase the amount of condition information that can be extracted from sleeper mounted accelerometers using advanced multibody simulation (MBS) models.

The developed condition monitoring framework provides a robust model-based identification of railway ballast support conditions, wheel–rail impact forces, and crossing rail geometrical irregularities, as well as closed form condition indicators computed directly from measurement signals. The presented analysis algorithms demonstrate resilience in handling extensive datasets, with the total acceleration database used for this thesis consisting of around three years of remote field recordings for eight crossing panels.

An essential signal processing technique presented in this thesis is an innovative method for reconstructing sleeper displacement. It relies on integrating acceleration in the frequency domain and using band-pass-based functions for detrending baseline distortion. Using these track displacements, an approach is demonstrated for independently observing the sleeper support conditions and the geometry of the crossing rail from a single measurement source by separating measured displacement into dynamic and quasi-static domains based on two distinctly determined track response wavelength domains.

The MBS investigations carried out in this thesis demonstrate a robust link between the condition of the crossing rail geometry, the contact force between the wheel and rail, and the proposed condition indicators that have been established based on the dynamic track responses. The MBS models serve as a basis for developing a procedure based on the Green's Kernel Function Method (GKFM) for an inverse identification of vertical wheel–rail contact forces and crossing rail geometry from measured sleeper accelerations. Additionally, this thesis demonstrates the possibility of determining ballast stiffness properties without prior knowledge of the crossing geometry, thus actually enabling the use of GKFM for inverse identification of wheel–rail contact force and crossing rail geometrical irregularity in a crossing panel equipped with a single sleeper mounted accelerometer.

In addition to measured sleeper accelerations, the geometry of the running surface of six crossings have been measured in situ using a laser scanner. These geometries have, together with measured wheel profiles, been implemented in the MBS models to account for a range of operating conditions.

Keywords: Switches & crossings, S&C, condition monitoring, multi-body simulations, MBS, wheel–rail contact forces, crossing rail geometry, condition indicators, embedded sleeper accelerometer, displacement reconstruction, Green’s functions, Green's Kernel Function Method, GKFM, inverse force identification

To the Poet, the Mathematician, and the Logos

Preface

The work presented in this thesis was accomplished at the Division of Dynamics at the Department of Mechanics and Maritime Sciences, Chalmers University of Technology, between February 2019 and May 2024 (part-time from May 2022). It was performed as part of the activities within the National Centre of Excellence in Railway Mechanics CHARMEC (CHAlmers Railway MEChanics, www.charmec.chalmers.se) within the project TS21 – "Model-based condition monitoring of railway switches and crossings". Parts of the research have been funded within the European Union's Horizon 2020 research and innovation programme in the Shift2Rail projects In2Track2 and In2Track3 under grant agreements No. 826255 and 101012456. The project has been supported by CHARMEC's industrial partners. In particular, the support from Trafikverket and voestalpine Railway Systems GmbH is gratefully acknowledged. The acceleration data used in this research was acquired with sensors from Konux GmbH and received via Trafikverket (the Swedish Transport Administration).

Acknowledgements

To my mentors, people who basically gave me some sort of life, a new me; that have found, developed, and opened my mind! There is not a word with which I can explain what I got in Gothenburg and Chalmers, but I can say with my heart: Björn!, Jens, Håkan, Arne, thank you!

To M2 Dynamics professors, colleagues, and friends: Anders, Roger, Peter F., Angela, Sinisa, Petri, Viktor, Thomas, Peter M., Magnus, Elena, Tore, Jim, Xin, Rostyslav, Mladen, Knut Andreas, Emil, Michele, Björn A., Ata, Pooria, Johan, Erik, Kourosh, Saptarshi, Sucheth, Anna-Lena, Carina, Pernilla, Jonas, Boban, it was a big pleasure meeting you, I hope climate change brings some benefits for you up there.

To my family: Dušan, Gordana, Strahinja, Jelena, Janja, Nikola, Luka, Anja, Sveta, Sonja, Stefan, thank you for your support, patience, and belief in me.

To my friends, from Novi Sad: k.Predrag, Ljubinko, Ivan, Nemanja, Milan B., Teodora, Viktor, Filip, Nikola Š., Maja, Bojan, Stefan, Nikola K., Sladjan, Ognjen, Miloš, Milan T., Aleksandar, Eli, Srdjan, Aleksej, Vasilije, Miodrag, Milan J., Jagoš, o.Petar, o.Velimir, o. Željko; from Delft: Uroš, Marko, Georgios, Arthuro, Vlad; from Gothenburg: Vladimir, Svetozar, o.Aleksandar, Nebojša, Branko, Miloš, Dalibor, Nikodim, Joca, Stefan, Predrag, Goran, Velimir, Puniša, Mladen, Bora, Mićo, Benkt, Stefan, Mile, Viktor, Nikolaj, Novče, Nenad, Mijo, Sanja, Ivana, Vesna B., Vesna V., Snežana, Stojica, Jelka, Mirjana, Nataša, Milena, v.Nektarije, o.Igor, Jefimija, Konstantin, Zorka, o.Dušan, Aleksa, Mihajlo, Slavica, o.Nemanja, o.Dragan, thank you for your love.

It is my honour to have this opportunity, in something important for me, to mention your names!

Additionally, it should be mentioned that the work with Green's functions whose results impressed us and hopefully others the most stems from the great mentorship of Björn. The idea came from him, the development and solution from me, and what in the end is given to the research community and industry from all of us together as a hard-working team.

Also, I want to share the snapshot of the most unique emotion in my heart that developed during my working days at Chalmers. It came from a long Swedish summer day, afternoon Sun rays lighting my office with the sound of sea gulls barking (like dogs, my hearing is not great), the smell of sea salt in the air and RHCP playing in the background (Californication) while reading a paper from Serbian Berkley professor Trifunac on acceleration integration and placing the foundation of all work I did at Chalmers. Those light rays and sparks that touched my heart felt like they were from the Uncreated Light, and that is one of the most important moments of my life. For the opportunity to be at Chalmers, I want to truly thank Sweden and the Swedish people and wish you all the best in the present and future.

Lastly, I would like to acknowledge Life, Love, Sacrifice, and Wisdom, ХВИМССРИОУГЖД.

Thesis

This thesis consists of an extended summary and the following appended papers:

Paper A Marko D.G. Milošević, Björn A. Pålsson, Arne Nissen, Håkan Johansson, and Jens C.O. Nielsen, On tailored signal processing tools for operational condition monitoring of railway switches and crossings, *Proceedings of ISMA2020 – International conference on noise and vibration engineering (online conference)*, Leuven, Belgium, September 2020, 15 pages

Paper B Marko D.G. Milošević, Björn A. Pålsson, Arne Nissen, Jens C.O. Nielsen, and Håkan Johansson, Reconstruction of sleeper displacements from measured accelerations for model-based condition monitoring of railway crossing panels, *Mechanical Systems and Signal Processing,* 2023, 192, 110225

Paper C Marko D.G. Milošević, Björn A. Pålsson, Arne Nissen, Jens C.O. Nielsen, and Håkan Johansson. Condition monitoring of railway crossing geometry via measured and simulated track responses, *Sensors,* 2022, 22, 1012.

Paper D Marko D.G. Milošević, Björn A. Pålsson, Arne Nissen, Jens C.O. Nielsen, and Håkan Johansson, Demonstration of a Digital Twin framework for model-based operational condition monitoring of crossing panels. *Proceedings of IAVSD 2021 –* The *27th IAVSD Symposium on the Dynamics of Vehicles on Roads and on Tracks (online conference)*, Saint Petersburg, Russia, August 2021, 10 pages

Paper E Marko D.G. Milošević, Björn A. Pålsson, Arne Nissen, Håkan Johansson, and Jens C.O. Nielsen, Model-based remote health monitoring of ballast conditions in railway crossing panels, *Proceedings of the 10th European Workshop on Structural Health Monitoring (EWSHM),* Palermo, Italy, July 2022, 11 pages

Paper F Marko D.G. Milošević, Björn A. Pålsson, Arne Nissen, Jens C.O. Nielsen, and Håkan Johansson, Inverse wheel–rail contact force and crossing irregularity identification from measured sleeper accelerations – A model-based Green's function approach, submitted for publication in *Journal of Sound and Vibration* (current status revised and resubmitted after minor revision decision), 2024, 34 pages

The appended papers were prepared in collaboration with the co-authors. The author of this thesis was responsible for the major progress of the work including taking part in planning the papers, developing the theory and the numerical implementations, running the simulations, and writing the papers.

Additional publications by the author:

1. Marko D.G. Milošević Towards model-based condition monitoring of railway switches and crossings, Licentiate Thesis, Department of Mechanics and Maritime Sciences, Chalmers University of Technology, Göteborg, Sweden, 2021

2. Björn A. Pålsson, Uwe Ossberger, and Marko D. G. Milošević, Calibration of a model for dynamic vehicle–track interaction in crossing panels to comprehensive field measurements, *The Fifth International Conference on Railway Technology: Research, Development and Maintenance,* Montpellier, France, 2022, 4 pages

3. Björn A. Pålsson, Henrik Vilhelmson, Uwe Ossberger, Michael Sehner, Marko D.G. Milošević, Harald Loy and Jens C.O. Nielsen, Dynamic vehicle–track interaction and loading in a railway crossing panel – Calibration of a structural track model to comprehensive field measurements, *Vehicle System Dynamics*, 2024, 27 pages, DOI: 10.1080/00423114.2024.2305289

Contents

Part I

Extended Summary

1 Introduction

1.1 Background and motivation

In a railway network the components that switch trains from one track to another are called switches & crossings (S&C, turnouts). This switching operation comes at a cost since S&C features load-inducing rail discontinuities that cause much larger deterioration rates compared to regular plain line tracks. Consequently, the high deterioration rates of S&C are the reason why railway infrastructure managers spend from tens to hundreds of millions of Euros annually on their maintenance. In Sweden, the annual maintenance cost for the around 12 000 S&C is estimated to 400 – 450 million SEK (~ 40 – 45 million EUR), which accounts for around 12% of the total maintenance cost [1]. In the United Kingdom, the corresponding cost in 2012 for the around 20 000 S&C was 189 million GBP (~212 million EUR), with an additional cost for renewals of 220 million GBP (~246 million EUR) [2]. As examples, Germany has a total of 69 983 (2014) S&C [2], France 25 600, and Switzerland 15 062 [3]. Since railway transportation is a very energy-efficient form of vehicle transportation with low environmental impact [4, 5], investments in it is a step towards a more sustainable society.

The current practice for S&C condition monitoring is by manual inspections in track using measurement templates and visual inspection. These inspections can be complemented with data from track recording cars. With digitalization and modern sensor technology however, it is becoming more and more feasible to equip track and vehicles with embedded sensors that can be used for continuous monitoring of e.g. S&C. The challenge that remains, however, is to link the measured responses to the physical state of the asset.

This situation provides a promising opportunity for implementing condition monitoring systems that have the potential to enhance maintenance decision-making, surpassing the capabilities of periodic manual inspections. This thesis addresses method developments towards such a system particularly focusing on support conditions in the crossing panel and crossing running surface geometry. It is built upon previous work within Chalmers Railway Mechanics Centre of Excellence (CHARMEC) [6-8].

1.2 Aim of research

The objective of this research was to develop a numerical technique based on physical and data-driven models that can effectively detect and predict the structural condition of S&C via acceleration data from embedded sensors. The project has focused on sleeper-mounted accelerometers which is an instrumentation technique used by several commercial actors. It appears to be the most practical sensor placement for long-term condition monitoring compared to an accelerometer mounted on the crossing rail itself. The goal was to ensure that the developed system is accurately providing understandable physical insights that can enable maintenance decisions and monitor performed maintenance impact.

The target system can be defined as a Digital Twin representation of the physical system, which integrates simulation models, condition monitoring data, and maintenance history to predict and detect maintenance requirements for S&C.

To this end the following developments have been completed and are presented in this thesis:

- Tailored signal processing tools for analyzing time and frequency domain properties of recorded accelerations, and quality assessment procedures for recorded signals and acquisition properties (Paper A)
- A set of techniques for robust signal processing of online condition monitoring data including a novel method for reconstruction of displacements from measured accelerations and extraction of qualitative crossing condition indicators (Paper B)
- A method that links the crossing geometry condition with processed operational condition monitoring data in the form of condition indicators validated by calibrated multibody simulations (MBS) models (Paper C)
- Framework for Digital Twin model and technique for detrending temperature impact on measured data, and a routine for automatised MBS model calibration (Paper D)
- Parameterised MBS ballast model and an automatic method for calibration of S&C MBS models based on remote condition monitoring data (Paper E)
- A Green's Kernel Function Method (GKFM) based procedure for an inverse identification of vertical wheel–rail contact forces and crossing rail irregularity from measured sleeper accelerations (Paper F)

In Figure 1 a flowchart is presented illustrating the link between the different papers.

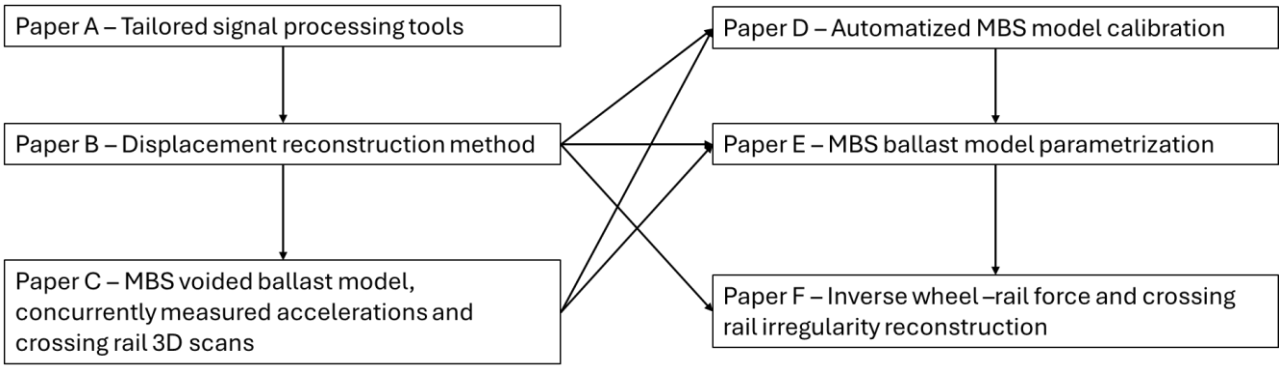

Figure 1 Flowchart of the link between the appended papers.

The end results of paper F are considered as the achieved goal of the developed condition monitoring system that based on measured accelerations provides physical insights of the ballast (calibrated MBS parameters) and crossing running surface condition (inversely identified irregularity), and enable making remote data-based maintenance decisions. The future work of this system concerns network level scaling, data fusion and data-based predictions.

1.3 Delimitations

The following are the main delimitations for the work presented in this thesis.

- The project has been limited to the use of data from existing sleeper mounted accelerometers.

- The project has been limited to the crossing panel. The methods are applicable also in the switch panel but would need more sensors along the track due to the longer transition zone between switch and stock rail compared to the wing rail to crossing nose, and an extension to lateral dynamics.
- The project has been focused on method development. While large scale implementation has been kept in mind, certain parts of the developed methods would have to be simplified or tabularised for computational efficiency in large scale implementation.
- The focus has been on condition monitoring using simulation models to leverage data. Prediction of future deterioration has not been considered.

2 Railway Switches and Crossings

2.1 S&C components

The layout of a standard S&C with a fixed crossing is presented in Figure 2. The main S&C components are the switch panel, closure panel, and crossing panel. In the switch panel, there are flexible switch rails that are actuated with the switching machines to shift position and thereby guide trains into the through or diverging routes. In the crossing panel, the arrangement of rails includes a crossing nose and two wing rails that allow for wheels to travel across the two intersecting routes. Further, there are check rails that impose a lateral constraint on passing wheelsets to prevent excessive lateral movement and derailment during the crossing transition. Traffic in the facing direction (move) goes from the switch panel towards the crossing panel, while traffic in the trailing move goes in the opposite direction.

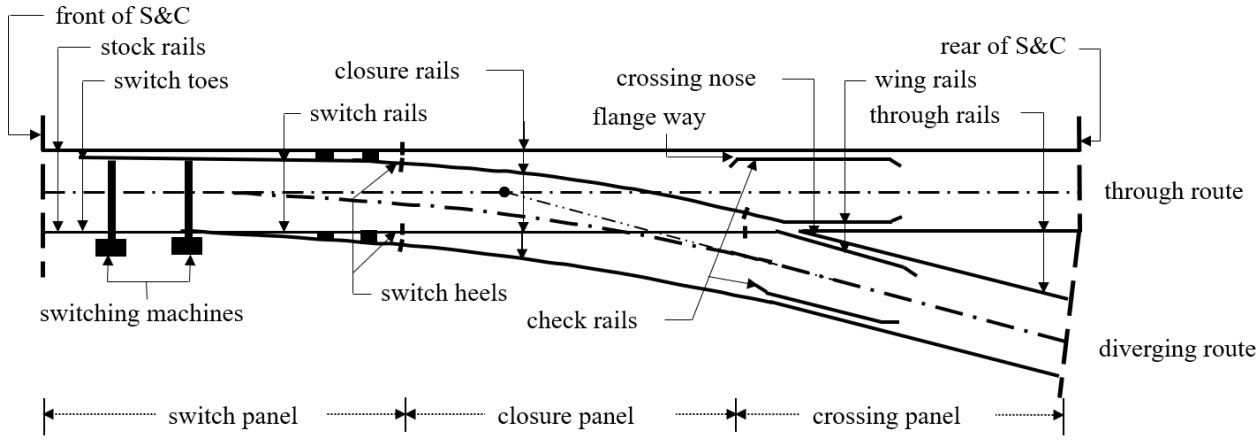

Figure 2. Layout, components, and nomenclature for a standard right-hand side S&C with a fixed crossing [9].

S&C can be installed on slab or ballasted track. This research is focused on the ballasted track form. The components of a ballasted track are grouped into superstructure and substructure [10], see Figure 3. The superstructure consists of rails connected with a fastening system to the sleepers. The substructure consists of the ballast, sub-ballast, and subgrade.

In general, ballast is an aggregate formed with crushed stones that forms the top layer of the substructure directly beneath the sleepers and supports the track superstructure. It provides track resilience and absorbs energy from the dynamic wheel–rail contact forces that are transferred through the sleepers. This crushed-stones-based solution provides efficient drainage and easy adjustment of track geometry during maintenance. Beneath the ballast lies the sub-ballast, which is a layer that prevents the mixing of ballast and subgrade. The subgrade is a platform consisting of placed soil and natural ground that creates a foundation for the ballast and superstructure. For further details on S&C design, see [7].

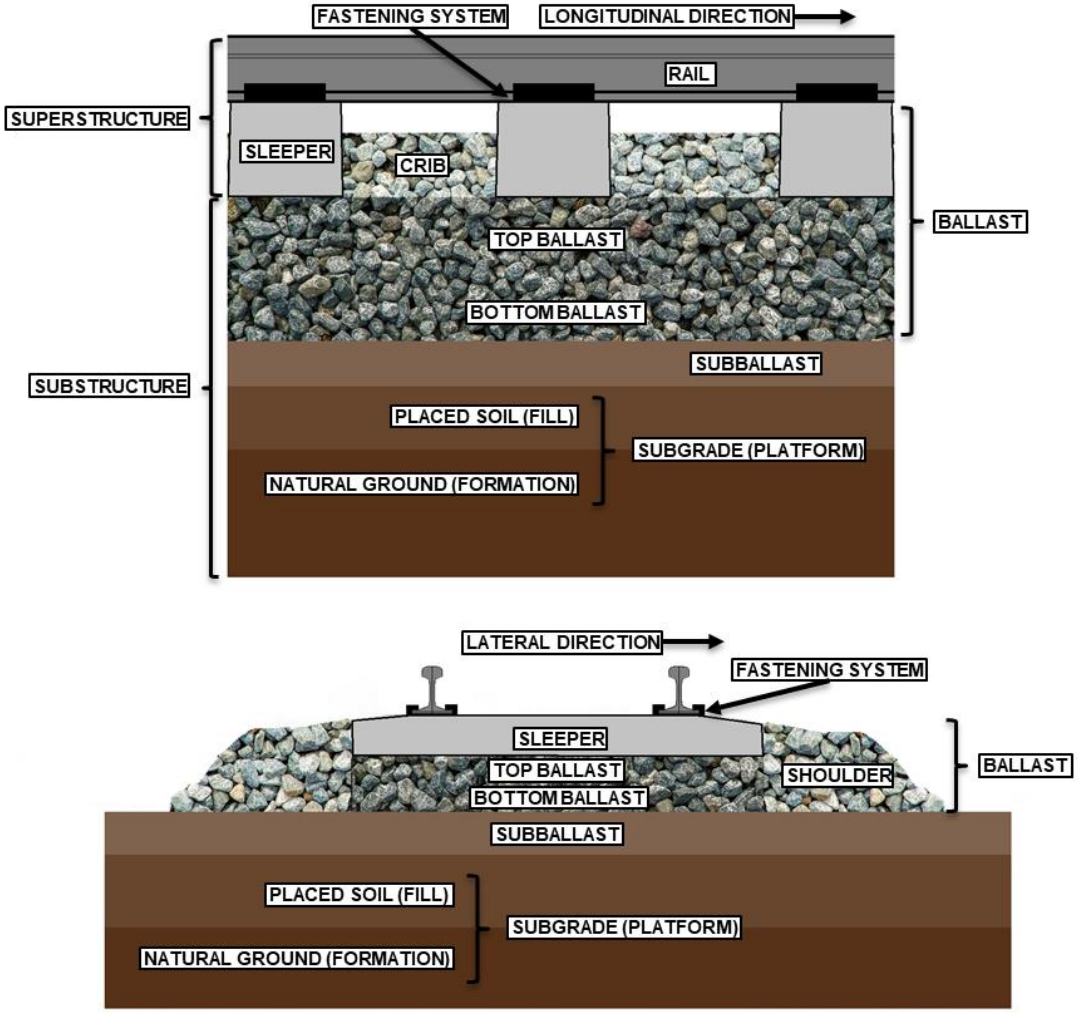

Figure 3 Longitudinal-vertical (top) and transversal (bottom) cross-sections of ballasted track. The nomenclature is based on [10].

2.2 Vehicle kinematics in railway crossing panels

This thesis focuses on the crossing panel in a S&C system. The primary crossing panel components are labelled, and the variations in contact conditions for passing train wheels are shown, in Figure 4. The illustration depicts a vehicle moving in the facing direction via the crossing panel along the straight route as indicated by the arrow at the bottom of the figure. The opposite direction of traveling is labelled as the trailing direction. The path that splits off to the right is the diverging route.

The wheel–rail cross-section in subfigures C and E illustrate the typical wheel–rail contact conditions experienced by the wheels on each side of the rail before the changeover. As the vehicle progresses towards the crossing, the right wheel will experience an impact force on the crossing nose when transitioning from the wing rail to the crossing nose (see detail D). This is caused by the change in the vertical movement of the wheel, transitioning from a downward motion when rolling on the wing rail to an upward motion on the nose. If the wheel has a concave tread due to wear, the transition happens at a later point (see detail B). This will typically result in significantly greater dynamic impacts

compared to a standard transition. The primary point of contact for the left wheel is consistent contact with the stock rail, although the inside of the wheel may also contact the check rail (see detail A). The check rail is a crucial guiding element that prevents excessive movement of the wheelset towards the crossing, hence avoiding any incorrect contact between the right wheel and the tip of the crossing nose.

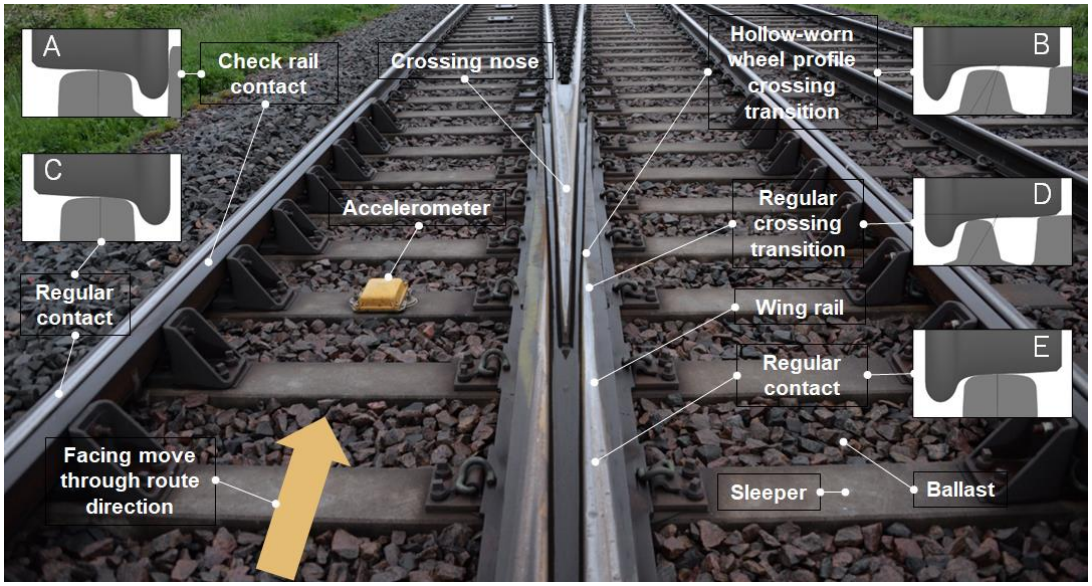

Figure 4 Illustration of a wheelset transition through the crossing panel with the nomenclature for the main components and illustration of wheel–rail contact conditions.

The main kinematic quantity behind the wheel–rail impact forces in a crossing panel is the trajectory of relative vertical wheel–rail displacement, see Figure 5 and Figure 6. Figure 5 shows a 3D scan of the crossing nose and wing rail, outlining a possible wheel path in the crossing transition, while Figure 6 shows extracted trajectories from MBS simulations using 19 different wheel profiles for three crossing panels ranging from good to severely degraded condition.

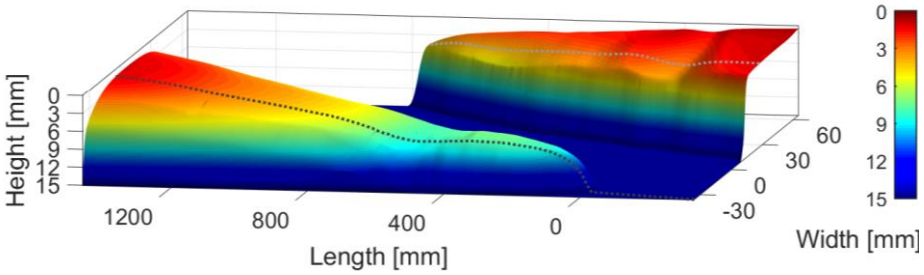

Figure 5 Crossing transition 3D scan, the crossing nose is to the left and the wing rail is to the right. The longitudinal dotted lines illustrate a possible wheel path in the crossing transition.

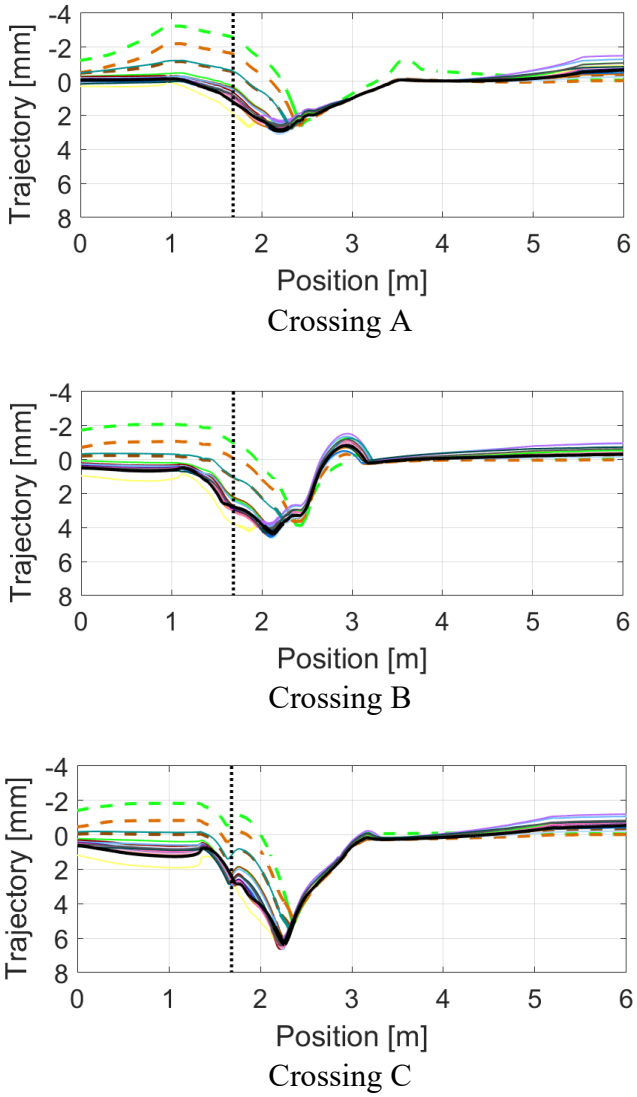

Figure 6 Extracted trajectories of relative vertical wheel–rail displacement for 19 different wheel profiles in three different crossings. The vertical dotted line indicates the position of the tip of the crossing nose, and the dashed lines are related to hollow worn wheels. Crossing A shows an example of a good state of crossing rail condition, while crossing C shows a degraded crossing rail condition with a large dip angle. Crossing B is an example of a medium state of a crossing rail condition with several kinks causing multiple wheel–rail impacts.

2.3 Vehicle–track dynamics in railway crossing panels

Figure 7 presents a cross-sectional view of a two-layer track structure model of the crossing transition. Starting from the top is the crossing rail. The rail is coupled to the sleepers via bushing elements that represent the resilience of the rail to sleeper connections. The sleepers in turn are coupled to rigid ground via bushing elements that represent the ballast and foundation stiffness. The figure also illustrates the location of the accelerometer shown in Figure 4. This accelerometer is permanently embedded in the track, and research in this thesis uses data acquired with this type of sensor.

When a wheel rolls over the crossing as in Figure 4 it excites the track in a broad frequency range. On the low end of the spectrum is the deformation stemming from the static wheel load. Further up in the frequency spectrum is the vertical wheel–rail impact load stemming from the designed discontinuity of the crossing. Based on analytical modelling, this force impulse is expected to consist of two main components [11]. The first is the P1 force (500 – 1000 Hz), which is due to the wheel and rail oscillating out of phase with a frequency related to the contact stiffness. The second is the P2 force, which is related to the wheel and track oscillating together on the foundation stiffness (50 – 100 Hz). Naturally, the dynamic response of the real structure can be expected to be broader with a wider range of excited frequencies. However, these analytically derived force components give an indication of the frequency regions of interest for typical system properties and are expected to qualitatively represent fundamental forces and frequencies that are present in the real system. In addition to the loads discussed above, there are rail surface irregularities at short wavelengths causing excitations at even higher frequencies. These dynamic loads cause damage to the crossing and the crossing panel structure. Over time each damage increment can accumulate to failures or deterioration leading to the need for maintenance.

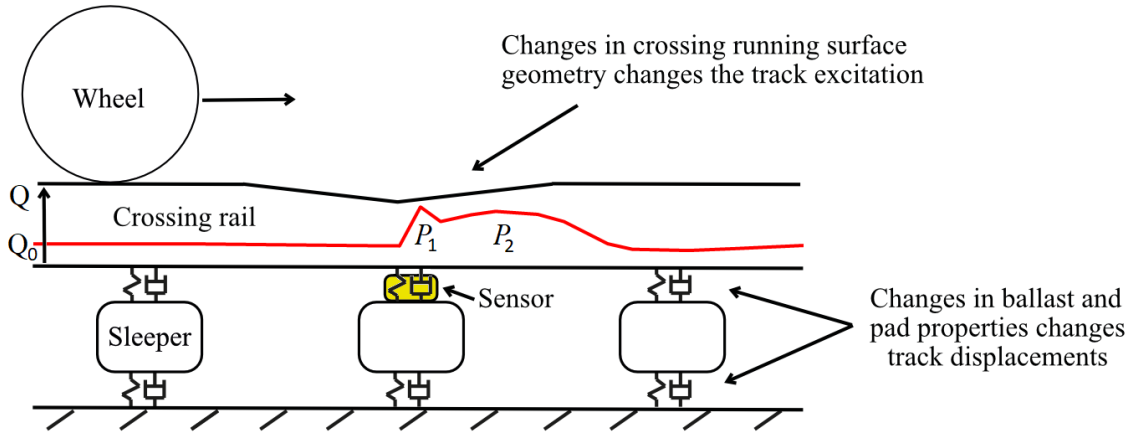

Figure 7 Schematic cross-sectional view in the longitudinal-vertical plane of a wheel rolling over the crossing transition, and illustration of P1 and P2 forces.

2.4 Railway crossings damage modes

The condition of a crossing panel is determined by its operational performance during a train passage. Two of the most dominant damage modes determining this condition are change of sleeper support conditions due to differential settlement and degradation of ballast,and crossing rail deterioration. Particularly the crossing rail deterioration can be observed on a surface level by observing the geometrical changes due to wear and plastic damage, and on the material inner rail level observing rail fatigue and cracks.

Condition monitoring methods addressing the condition of the unloaded crossing panel can be found in the literature [12, 13]. These are particularly used for addressing cracks and fatigue. Crossing panel condition monitoring may also be performed with an axle box accelerometer [14]. This addresses operational crossing panel behaviour but with a limitation to a specific type of train wheels, axle loads, restricted train speeds, and no ability to address the global ballast deformation patterns. A sleeper acceleration-based method for crossing panel condition monitoring can meet the two worlds and address

both the ballast and the crossing rail condition in the crossing panel, in a fully operational condition environment.

From a global perspective, the condition of the track in the crossing panel is governed by track geometry and support conditions. An important contributor to irregularities in track geometry are permanent displacements due to differential track settlement [7]. The geometric irregularities can cause higher wheel–rail contact forces that cause higher degradation rates. In addition, voids can form between sleeper and ballast resulting in higher dynamic rail and sleeper displacements, see Figure 8. The possible maintenance actions for addressing track geometrical irregularities due to track settlement and sleeper voids are tamping and stone blowing [15].

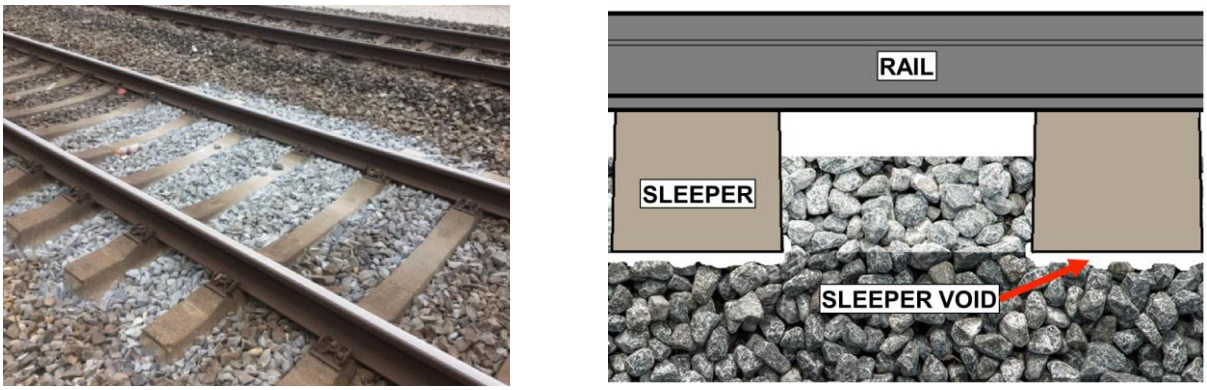

Figure 8 (a) White spots of ballast breakdown due to voided sleeper [16], the picture is courtesy of Prof. Mykola Sysyn. (b) 2D longitudinal cross-section illustration of sleepers with a void.

On a more local level, the condition of the crossing panel is deteriorated by crossing rail plastic deformation, wear, and rolling contact fatigue, see Figure 9. These damage modes directly influence crossing transition kinematics and the resulting dynamic wheel–rail contact forces. Maintenance in case of such damage modes is grinding/milling, welding repairs, or complete rail replacement. It is important to mention that poor welding repair can leave the crossing rail in a generally degraded and dangerous state. For a review on common material degradation mechanisms in S&C, see [17, 18]. High wheel–rail contact forces at the crossing panel transition can also be induced by poor wheel tread conditions, see Figure 10. Additionally, it is interesting to mention that a new crossing is subjected to an initial plastic rail deformation due to an adaptation to the passing of multiple wheel profiles [19]. This means that the newly installed crossing rail does not have an optimised running surface geometry.

(a) (b) (c)

Figure 9 Crossing nose degradation states: (a) plastic deformation, (b) wear, (c) rolling contact fatigue. Pictures are courtesy of voestalpine Railway Systems GmbH.

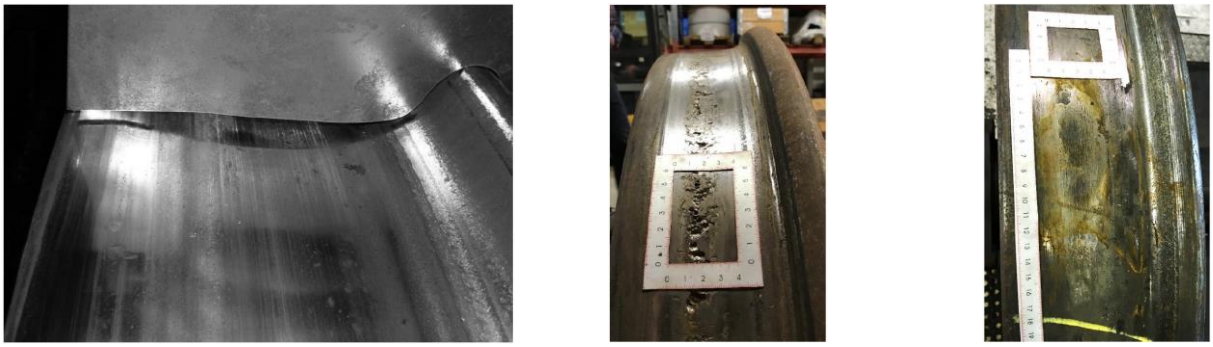

(a) (b) (c)

Figure 10 Wheel tread degradation states: (a) hollow worn wheel, (b) severe rolling contact fatigue, (c) long wheel flat. Pictures are courtesy of Prof. Anders Ekberg (a) and PhD Michele Maglio (b,c).

3 Model-based condition monitoring of switches & crossings

This chapter presents a background on the modelling and simulation of dynamic vehicle–track interaction in S&C as well as previous work on condition monitoring. It ends by presenting the Crossing Panel Condition Monitoring (CPCM) scheme developed in **Paper F** that is the main outcome of the thesis.

3.1 Digital Twin landscape

Digital Twins for condition monitoring of mechanical systems are typically physics-based (white-box) or machine learning-based (black-box) [20]. This dichotomy is illustrated with the Digital Twin landscape presented in Figure 11. For the physics-based systems, the Digital Twin has deep domain knowledge defined by Newtonian mechanics. For condition monitoring applications, one of the main goals is to make service life predictions. This can be achieved with models that simulate operational conditions and damage evolution. The limitations of this white-box approach are model uncertainties, overall model capabilities, and potentially high computational costs. On the other hand, machine learning-based Digital Twins are governed by data science and the data model does not have physical domain knowledge. The advantage of this method is robustness in the sense that the analysis algorithm gets input and produces output without user interaction. Also, the model can improve over time if it is continuously trained with new data. However, the training data sets must be obtained, and the model cannot operate reliably outside the training domain, which typically does not cover changes in operational conditions and more importantly the outlier events. Thus, the machine learning approach cannot predict failure cases for which it is not trained. In general, machine learning algorithms either perform well (trained domain) or catastrophically fail (outlier events).

To this end, the research carried out in this thesis is operating within the physics-based Digital Twin domain. Considering the presented landscape, it is foreseen that the two solutions should be joined in future work such that the limitation of one method can be compensated with the capabilities of the other. This could be achieved by, for example, simulating operational conditions on damaged S&C (outlier events) and training the machine learning algorithms with this synthetic data.

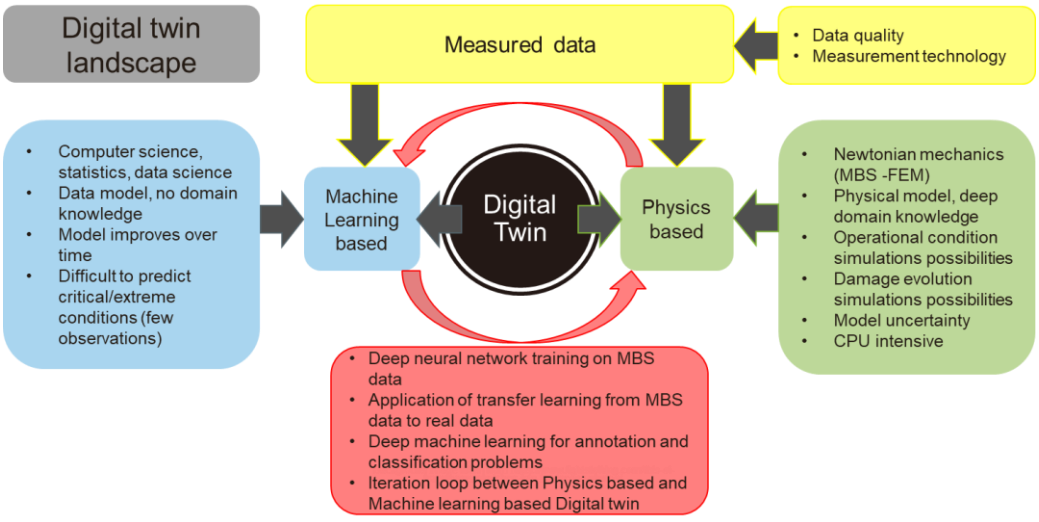

Figure 11 Digital twin landscape for condition monitoring of S&C system.

3.2 Related work

This subsection presents a literature survey addressing three different areas covered in S&C-related research: experimental analysis and instrumentation (sensors), numerical analysis, and general condition monitoring related research

3.2.1 Experimental work

On the experimental side, [12] uses ultrasonic guided waves for active structural health monitoring of S&Cs. The authors claim that the method can detect growing defects (cracks) in real-time, but not the existing ones. This contrasts the sleeper embedded accelerometer sensing that is used in this thesis that cannot address defects on crack level, but it can address both growing and existing defects through operational dynamic response of a crossing and employment of the MBS model. Further on the smaller defect level, in [13] the authors used image processing and machine learning to assess magnetic particle images for the prediction of rolling contact fatigue in crossings.

In [21], two experimental tools are used to measure the dynamic response of a railway crossing. An ESAH-M system with a 3D accelerometer and speed detector and Video Gauge System for dynamic displacement recording of rail or sleeper. In this work, a so-called “fatigue area” criterion is set for damage assessment of the crossing nose. The derived criterion can also be addressed with the crossing irregularity condition feature from this thesis by accumulating information of the impact location from a longer time window of monitoring.

In practice, track measurement cars [22] are often used for monitoring of track irregularities, but they can experience difficulties in measuring irregularities in S&C due to the varying rail profiles as they use automatised algorithms based on the gauge and regular stock rail profile which experience distortions from the discontinuities present at the crossing panels. Additionally, instrumented wheelsets [23] can be used to measure wheel–rail contact forces, but this is mostly employed for research purposes of crossing panel condition monitoring.

For the aspect of addressing long-term condition monitoring, two-dimensional (2D) cross-sections of a crossing rail have been recorded at 19 positions over 30 months in intervals of three to six months [19]. By applying a statistical method of filter-based prognostics using track irregularities as input, a prognostic tool for railway track degradation was proposed and demonstrated for four S&C [24].

On the instrumentation side, an overview of the implementation of geophones, accelerometers, and 3D-scanners for S&C monitoring was presented in [25]. Accelerometers and remote video monitoring were used in [21] to resolve crossing rail displacements. In [26], micromechanical system (MEMS) accelerometers are studied in the context of S&C maintenance.

3.2.2 Numerical work

In the literature, there are a plenty of studies that concern simulations of dynamic vehicle-S&C interaction. Results from MBS simulations typically demonstrate good agreement to measurements where those are available. In [27], dynamic vehicle–track interaction and loading in a crossing panel is studied with the use of comprehensive field measurements which include six ballast pressure sensors on the crossing sleeper, eight sleeper accelerometers, one accelerometer on the crossing rail, five strain gauges on the crossing sleeper, and three strain gauges on the crossing rail. The work demonstrated a calibration routine for an MBS model and good agreement to measurements after ballast voids had been accounted for. The MBS model was developed to allow for holistic assessment of S&C

performance in a so-called Whole System Model scheme. In [28] the Whole System Model approach is employed to predict damage in S&C.

Two different S&C FE models are investigated and validated with field measurements in [29]. The first model uses detailed MBS model with simplified FE model of the track, while the second uses dynamic forces from the first model applied to a detailed FE model.

In [30] a comparison is made for co-running, finite element, finite element in co-simulation, and modal superposition based model track models for the simulation of dynamic vehicle–track interaction in switches and crossings. The study shows that all models can provide good agreement for the simulation of the dynamic wheel–rail interaction forces. Co-running model and modal superposition model have low computational cost with the drawback of not resolving the track response below the rail level (co-running) and not having the non-proportional damping in the model (modal superposition). FE-based models have significantly higher computational cost but can incorporate higher modelling detail, and are generally incorporated in the MBS software [27], coupled to the MBS code with a co-simulation scheme where vehicle and track are modelled in different software and coupled in the time domain [31], or just subjected to a moving load [32] (ussualy for detailed 3D FE modelling cases). On the side of less computationally demanding models, co-running models use an equivalent system of masses and bushing elements under each wheelset that moves with the vehicle [33], and modal superposition models use eigenmodes from a reference FE model to represent track flexibility [34]. Additionally, a modal substructuring approach can be made to decrease computational cost of complex FE models [35, 36].

The CHARMEC competence centre at Chalmers has carried out three PhD projects in recent years on the optimisation of S&C [6], wheel–rail impact loads and track settlements in railway crossings [7], and long-term damage evolution in railway crossings [8]. The MBS model employed in this thesis presents a continuation of the models developed in these theses, particularly continuing on the developments from [6].

For an comprehensive surveys on track modelling, focused on plain line track, see [37].

3.2.3 Condition monitoring related research

A thorough review of vibration-based damage detection in civil structures is presented in [38]. It overviews traditional methods (58 articles) as well as Machine Learning and Deep Learning methods (54 articles). It is stated that the most successful damage detection systems are those used for vibration-based condition monitoring of rotating machines. The high efficiency of damage detection for such systems lies in the controlled operational environment and the minimal influence of environmental conditions.

For example, feature extraction can be a basis for fault detection [39]. It is usually carried out in the frequency domain by identifying and observing changes in eigenfrequencies and eigenmodes of the structure. This can be approached as a black-box type of condition monitoring system with a binary outcome (healthy or damaged) and damage index, or as a white-box condition monitoring system by observing the evolution of physical damage. In addition, these two approaches can be combined, and such systems are referred to as grey-box condition monitoring systems.

On the structural health monitoring side, notable work in the domain of operational modal analysis and stochastic subspace system identification can be found in [40-42]. Those types of methods rely on the assumption that the system excitation is random and provide as a result identified system properties such as eigenfrequencies and eigenmodes which are further used for fault diagnosis.

As a general view of S&C and its maintenance, the PhD thesis [3] presents modelling of degradation processes of switches & crossings for maintenance and renewal planning. Also, a comprehensive study

on railway S&C monitoring is presented in the PhD thesis [2], addressing life-time monitoring of in-service switches and crossings through field experimentation. It was concluded that the rate of change of S&C geometry is the key contributor to the development of S&C condition monitoring knowledge. To apply a condition monitoring system to railway crossing panels, which are subject to varying unknown loads and are highly sensitive to environmental conditions, it is prudent to prioritize the initial stages of system development on identifying distinct damage signatures and obtaining a clear physical understanding of their impact on the dynamic response that is monitored. Incorporating resilient feature extraction methods may be considered during further phases of development, once the specific type of damage and the precise means of capturing its distinctive characteristics have been determined.

3.3 Condition monitoring framework

In this thesis, the developed Crossing Panel Condition Monitoring (CPCM) method focuses on the monitoring of two damage modes: the degradation of crossing rail geometry and the degradation of ballast support conditions. A flowchart of the CPCM scheme is presented in Figure 12.

The steps of the CPCM are as follows:

- Measurements of sleeper acceleration and obtaining information on the type of S&C.
- Based on the measured accelerations, reconstruction of displacements using the method from **Paper B**.
- Employing a multibody simulation model that incorporates a FEM structural track model for ballast parameter calibration and identification. The calibration is based on reducing the discrepancy between the measured and simulated sleeper displacements during the passage of one train bogie as described in **Paper E**.
- Identification of vertical wheel–rail contact forces during the wheel-crossing transition. This is achieved by linking the vertical sleeper displacements and wheel–rail contact forces using GKFM [43-47], as presented in **Paper F**.
- Calculation of wheel and rail displacements during the crossing transition based on the identified wheel–rail contact forces and GKFM, which link moving point rail displacement and wheel–rail contact forces (**Paper F**).
- Identification of crossing irregularity, which refers to the relative vertical trajectory when the wheel rolls over the crossing transition. This is done by subtracting the vertical displacement of the rail from the vertical displacement of the wheel (**Paper F**).

In conclusion, the CPCM system outputs ballast stiffness, wheel–rail contact forces, and crossing irregularities as condition indicators. By monitoring the evolving indicators, the degradation of the crossing panel over time can be assessed.

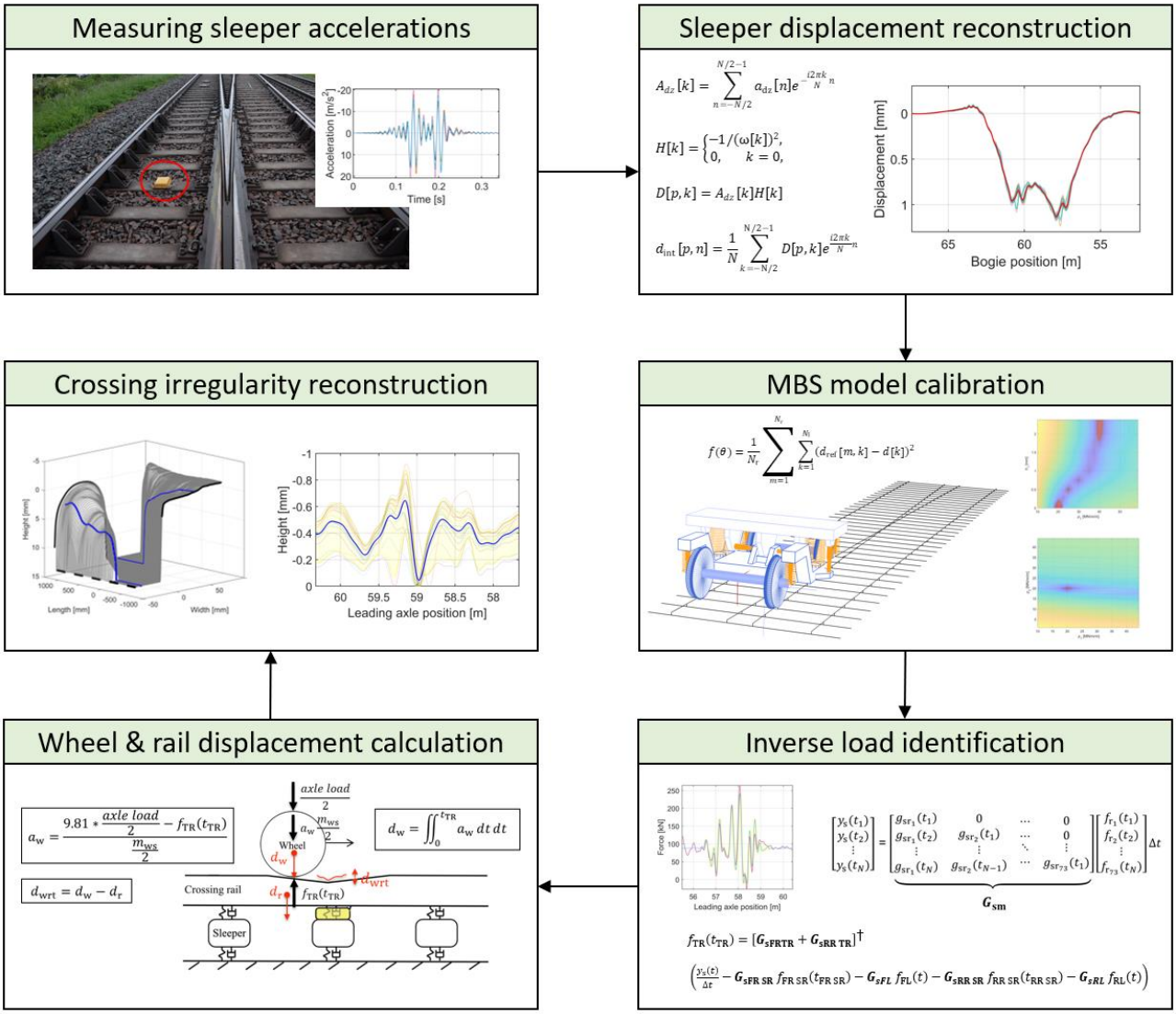

Figure 12 Crossing Panel Condition Monitoring system framework

4 Data used in the project

The field measurement data used in this research includes 3D scans of crossing rail geometry and acceleration measurements obtained with a permanently embedded sleeper sensor (shown in Figure 4).

4.1 Crossing rail geometry scans

Crossing rail geometry scans have been performed for six crossing panels at three locations on the southern mainline in Sweden. Details for the given crossing panels are presented in Table 1. The design differs between the two locations. In Höör, the latest generation of S&Cs (60E) featuring rail fastenings with a soft resilient element (rail pad) between crossing rail and sleepers is installed, while Stehag and Vätteryd feature an older design (UIC60) with a direct and very stiff connection between crossing rail and sleepers.

The geometries were scanned using the high-precision Creaform HandySCAN 3D laser scanner, see Figure 13. During the in-situ scanning, additional reference objects were mounted on the crossing rail to increase the quality of the scan. The properties of the scanner are given in Table 2. Examples of a processed geometry scan and prepared 2D crossing rail profiles for MBS analysis are given in Figure 14 and Figure 17.

Table 1 Crossing panel data.

Location	Höör	Höör	Stehag	Stehag	Vätteryd	Vätteryd
Crossing name	21B	22A	21A	21B	102	131
Design	60E 1:18.5	60E 1:18.5	UIC60 1:18.5	UIC60 1:18.5	UIC60 1:18.5	UIC60 1:18.5
Direction	Trailing	Facing	Facing	Facing	Trailing	Facing
Radius	1200 m	1200 m	1200 m	1200 m	1200 m	1200 m
Crossing rail installation date	2014	2014	2018	2012	2014	2014
Scanning date	2019-06-04					

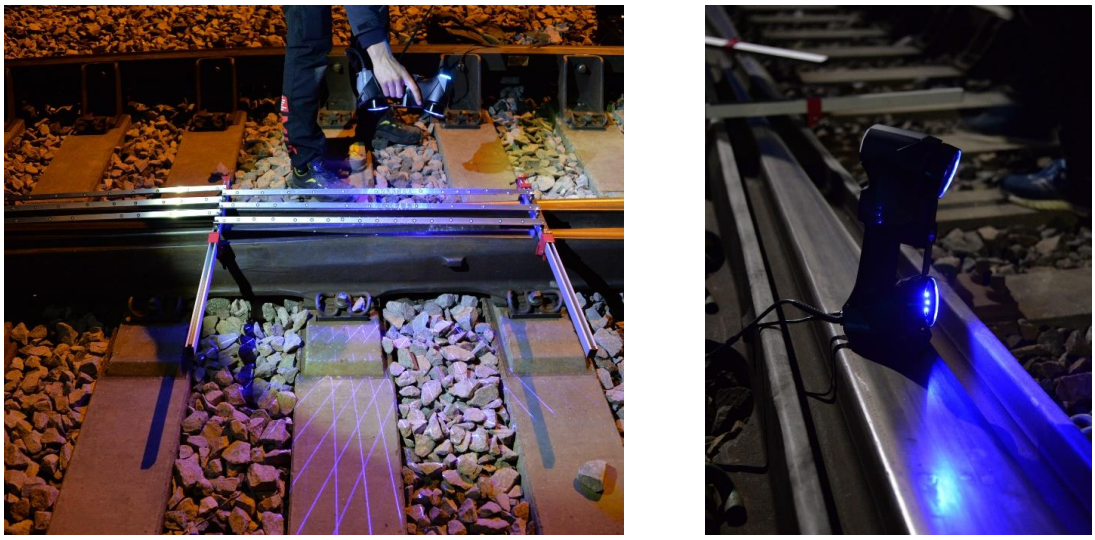

(a) **(b)**

Figure 13 (a) 3D geometry scan of a crossing rail, (b) Creaform HandySCAN 3D laser scanner [48].

Table 2 3D scanner properties.

Scanner information	
Device	Portable 3D laser scanner
Accuracy	0.035 mm
Volumetric accuracy	0.02 mm + 0.06 mm/m
Measurement resolution	0.025 mm
Mesh resolution	0.1 mm
Measurement rate	800 000 measurements/s
Light source	7 laser crosses
Scanning area	310 x 350 mm

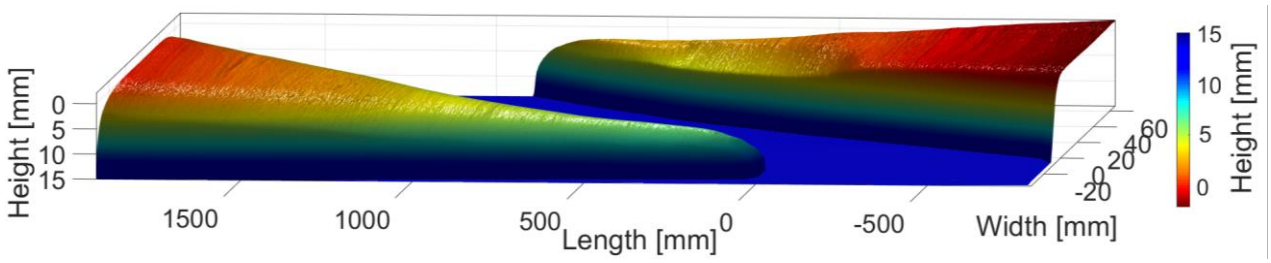

Figure 14 3D scan of crossing nose (left) and wing rail (right).

4.1.1 3D scan processing

To incorporate scanned geometry in MBS software, a sequence of 2D cross-section profiles needs to be created from the point cloud scan output. One example of raw data from the 3D scan of the VAD

131 crossing is shown in Figure 15. In the figure, holes in the surfaces can be observed and there are also outlying geometry points due to measurement noise.

Steps taken to prepare the scanned geometry for MBS simulations are as follows:

- Detection and removal of outlying data points with a fine point distance tolerance for meshing surfaces
- Orienting the geometry in space to the defined reference frame of the MBS, see Figure 16
- Interpolation of cloud point data to a specified horizontal grid (nearest-neighbour method [49] with 0.1 mm horizontal and 1 mm longitudinal spacings)
- Smoothening of the data with two decoupled moving average filters (2 mm lateral and 20 mm longitudinal filter lengths)
- Sampling the data to 2D profiles with a specified longitudinal spacing (chosen longitudinal spacing 10 mm)

Figure 17 shows post-processed 2D cross-section profiles ready for MBS analysis. The 10 mm longitudinal spacing was found to be sufficient as a finer discretisation did not alter the simulation results up to 1000 Hz when observed in the frequency domain.

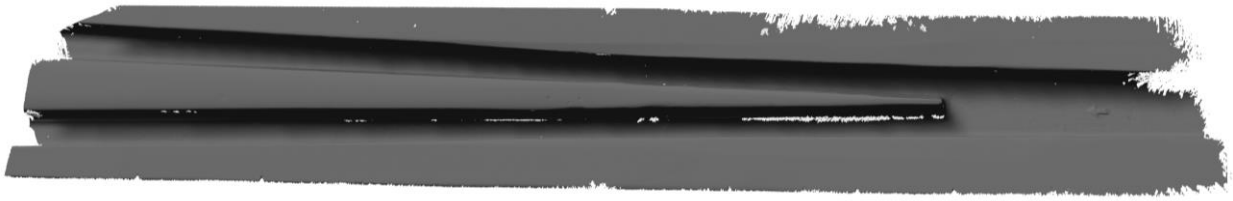

Figure 15 Example of raw 3D geometry scan, crossing panel VAD 131.

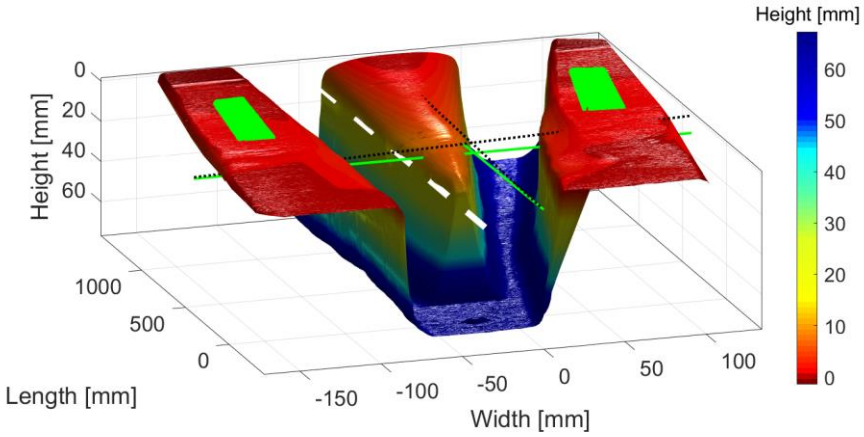

Figure 16 Example of geometry alignment reference surfaces and axes.

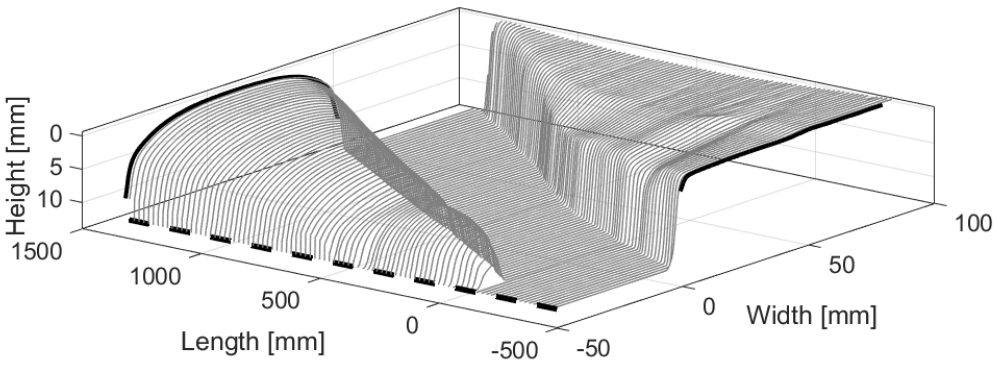

Figure 17 Post-processed 2D cross-section profiles prepared for MBS analysis. The longitudinal spacing between profiles is 10 mm. The crossing nose is on the left and the wing rail is on the right.

4.2 Sleeper acceleration measurements

Two datasets of sleeper acceleration are used in the presented research. The first dataset was obtained during four months of monitoring of eight crossing panels, from September 2017 to January 2018. This dataset contains approximately 100 000 train passages. The second dataset concerns six crossing panels and a monitoring period from June 2019 till May2022.

The acceleration data was acquired with sensors from Konux GmbH, permanently mounted on the sleeper next to the crossing transition (shown in Figure 4). All presented studies used raw data directly from the sensor, for which the properties are given in Table 3.

Table 3 Konux GmbH Accelerometer properties.

Sensor information	
Device	Monoaxial cellular accelerometer
Installation	Permanent sleeper connection
Direction of measurements	Vertical
Sampling rate	2 kHz or 20 kHz
Range	±50g and ±100g

4.3 Wheel profiles

A set of scanned wheel profiles has been used in this thesis. The set consists of a nominal S1002 profile, 15 measured profiles from Swedish Regina passenger trains [50], and three measured hollow worn wheel profiles [51]. From these profiles, the nominal S1002 and the Regina profiles are expected to be the most representative of the profiles present on X2 trains. The hollow worn profiles were included to illustrate their effect on the wheel–crossing interaction but are more commonly found on freight wheels that see less frequent maintenance. The Regina profiles have been sampled from a larger set of 279 profiles to save simulation effort. The 15 profiles uniformly cover the range of global cone angles (φ) present in the original sample, where φ is defined as the height difference between the

flange root and the field side of the wheel profile normalised by their lateral spacing [52]. By ensuring a large and uniform spread in φ available from the wheel profile sample, the broadest possible range of transition locations will be evaluated for the measured crossing geometries.

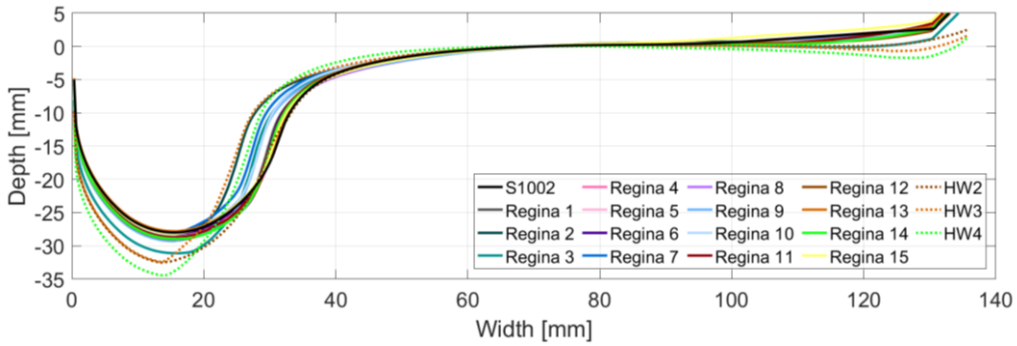

Figure 18. Wheel profile set used in the MBS analysis. Nominal wheel profile S1002 is marked with black colour, scanned Regina passenger train wheel profiles are marked with continuous coloured lines, while the three hollow worn wheel profiles are marked with dashed lines.

5 Methods of the project

The following chapter provides a summary of the key, used and developed, methods of this thesis.

5.1 Simulation model

To improve the understanding of the measured data, the dynamic vehicle–track interaction in the crossing panel is modelled and simulated using multi-body simulations (MBS). The analyses are performed with the commercial software Simpack (v.2019). A 3D view of the model is presented in Figure 19. The track model is a finite element model with all the rails and sleepers described by Timoshenko beam elements that are condensed to so-called super elements using the Craig-Bampton method [53]. The condensation reduces the size of the underlying finite element model, but primarily the method was used as this is the input format required for flexible track structures in Simpack. The node spacing of the super elements is presented in Table 4, while the node spacing in the original FE model is half of that. The crossing is at the longitudinal centre of the track model. Each sleeper is supported by a discretised system of independent bushings (springs and viscous dampers) in the vertical direction that represents the ballast (Winkler bed). Each connection between the sleeper and rail is modelled by a single bushing element representing the rail fastening. The nodes of the rails and sleepers are partially constrained to reduce model size. Here, the sleeper nodes can displace vertically, while the rail nodes can displace vertically and laterally including the corresponding rotations. In total, the number of degrees of freedom of the track model is 2026. The model is generated with an S&C model generation script [54] and implemented in Simpack using its non-linear flextrack functionality. See [55] for a thorough evaluation of numerical approaches for simulating train–track interaction in S&C.

A convergence study has been performed concerning the required length of the track model to save computational effort while maintaining accuracy. The study started with a track model of 100 sleepers in length. For different lengths of the model, sleeper, and rail accelerations were compared in the region ±6 m from the crossing transition. For the present investigation, it was found that a track model of 21.6 metres in length (37 sleepers) is sufficient for simulating the 12 metres (±6 m) of single train bogie passage over the crossing transition (in facing and trailing moves). The vehicle is modelled as a single bogie according to the passenger vehicle model from the Manchester benchmarks study [56], but with adjusted mass properties to correspond to the axle loads of the X2 train cab car bogie (15.5 tonnes). The input to the MBS model is presented in Table 4. The crossing rail geometry in the simulations is represented by 2D profiles discretised from the 3D scans of the crossing rail, or from a nominal generic crossing from the S&C benchmark study [57] that is used here as a reference case. The software builds a 3D rail geometry from the 2D sections via a cubic spline interpolation. A 10 mm longitudinal profile spacing is used in the transition area between the crossing nose and wing rail. An equivalent linearised Hertz contact is used for the normal wheel–rail contact, while FASTSIM [58] is used to model the tangential contact. A 2D cross-section of the vehicle–track model is shown in Figure 20.

Table 4 Nominal MBS parameter values.

MBS model components		Value
Vehicle	Type	Single bogie [56]
	Wheel profile	S1002
	Wheel radius [m]	0.46
	Wheelset mass [kg]	1340
	Axle load [kg]	15 500
	Axle spacing [m]	2.9
Rail*	Element type	Timoshenko beam
	Node spacing along body in Simpack [m]	0.3
	Profile	UIC60/60E1
	Young's modulus [GPa]	210
	Mass density [kg/metre rail]	60
	*The crossing rail is modelled as having three times the bending stiffness and mass of the standard rail	
Rail pads	Element type	Kelvin bushing elements
	Vertical stiffness [MN/m]	120 (Nominal) 60 (60E1 design) 1200 (UIC60 design)
	Vertical damping [kNs/m]	25
Sleeper	Element type	Timoshenko beam
	Node spacing along body in Simpack [m]	0.25 average
	Young's modulus [GPa]	30
	Mass density [kg/m^3]	2 400
Ballast	Element type	Kelvin bushing elements
	Vertical stiffness [MN/m/m]	30
	Vertical damping [kNs/m/m]	125

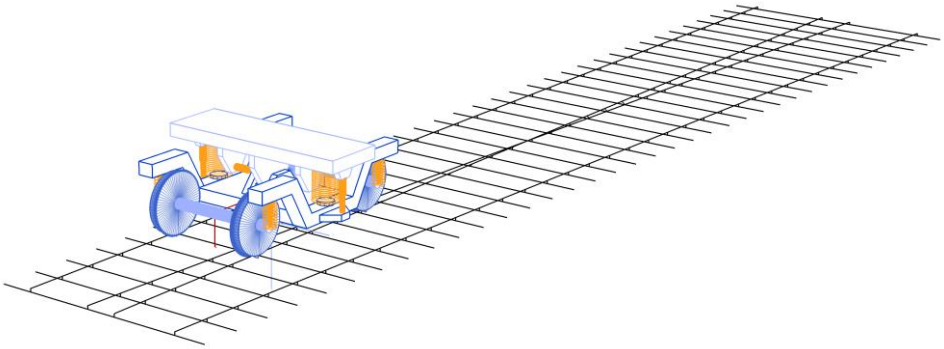

Figure 19 MBS model of vehicle–track system (Simpack v.2019).

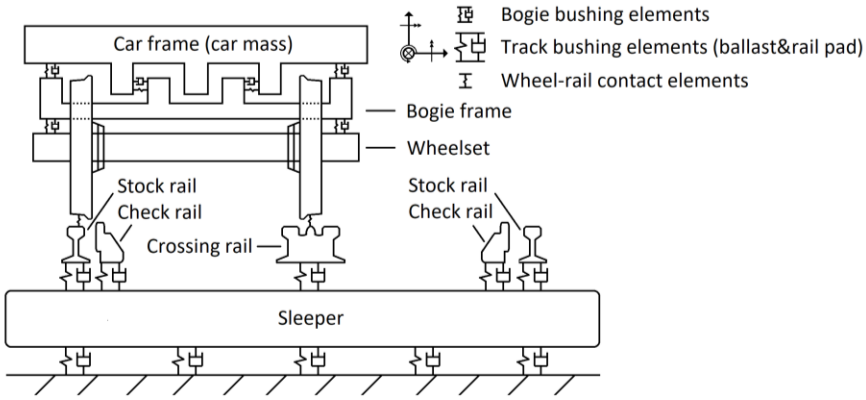

Figure 20 2D representation of vehicle–track system during a passage through the crossing panel.

5.2 Signal processing

The signal processing methods used in this thesis mainly address filtering and observations in data trends. In the process of choosing an optimal filtering technique, various finite impulse response and infinite impulse response filters have been employed **Paper A** The investigation led to the conclusion that the most stable and controlled filtering performance is achieved with ideal brick digital filters and frequency domain-based filtering. This particularly showed to be robust for addressing very low high-pass frequencies to resolve drifts and distortions in integrated displacement signals. It is argued that the applied band-pass filters and optimised frequency ranges are one of the main developments of this thesis when related to the separation of ballast and crossing rail influence on the crossing panel dynamic response.

Concerning the long-term trends, data is processed mainly based on moving average windows avoiding overfitting or underfitting the data with possible statistic models. Further, the developed condition monitoring indicators are based on a combination of band-pass filters and moving average windows supported by MBS results that include operational conditions. Additionally, the processing of scanned crossing geometries involved 2D moving average windows for addressing the noise in the scan data.

5.3 Condition monitoring indicators

By combining measurements with an MBS model (for validation and physical insight), a crossing condition indicator $C_{\lambda_1-\lambda_2,\gamma}$ is derived in **Paper B**. The indicator is defined as the root mean square of a track response signal γ that has been band-pass filtered between frequencies corresponding to track deformation wavelength bounds of λ_1 and λ_2 for the vehicle passing speed ($f = v/\lambda$). In this way, the indicator ignores the quasi-static track response with wavelengths predominantly above λ_1 and targets the dynamic track response caused by the kinematic wheel-crossing interaction governed by the crossing geometry. For the studied crossing panels, the indicator $C_{1-0.2\ m,\gamma}$ ($\lambda_1 = 1$ and $\lambda_2 = 0.2$) is evaluated for $\gamma = u$, v or a as in displacements, velocities and accelerations, respectively. Example results for six crossing panels showing the relation between the derived condition indicators and wheel–rail contact force can be seen in Figure 21.

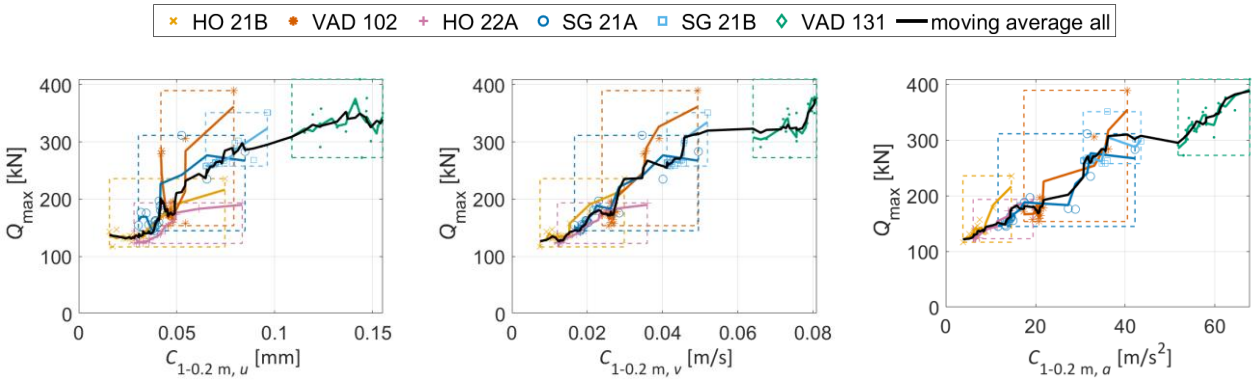

Figure 21 Relation between simulated $Q_{\max}$ and $\boldsymbol{C_{1-0.2\ m,\gamma}}$ for six different crossing panels with calibrated track parameters. The black continuous line presents a 7-points moving average filter through the cloud of all scatter points.

5.4 Optimisation routines

The optimisation routines employed in this thesis are related to finding an optimal high-pass frequency in the displacement reconstruction, re-orienting scanned rail geometry with respect to reference surfaces and gauge lines, and model calibration procedures.

In general, linear and nonlinear least-squares solvers are used, with some sensitivity studies being based on a brute force approach. The model calibration routines are defined as multi-parameter problems based on fitting either single reconstructed displacements or objective functions based on weighted accelerations, velocities, and displacements.

5.5 Displacement reconstruction

In this subsection, the developed **Paper B** methodology for sleeper displacement reconstruction from sleeper acceleration is presented. The methodology is based on frequency-domain integration, optimisation of the high-pass filter pass frequency, and a reconstruction relative to the "at rest position" (that is defined as the zero-displacement state located before and after the train bogie passage). The full reconstruction is performed in five steps. In the following description of each step, the equations that

concern the convolution and cross-correlation operations are written in continuous form, while the equations concerning the Discrete Fourier Transform (DFT) are given in discrete form.

Step 1. The acceleration recording from one full train passage is pre-processed to identify the segments of the signal that are located between each pair of bogie passages. Initially, the acceleration recording a_{d} with time duration T is quadratically detrended. Further, each element of a_{d} is squared and spatially convolved with a 2-metres moving average filter $f_{2\mathrm{m}}$ (see $f_{2\mathrm{m}}$ in Eq. (1) and Eq. (2)). In Eq. (2), M is a signal duration corresponding to a spatial length of 2 metres (determined from the train speed). Finally, the segments of a_{d} located in-between bogie passages (here denoted s_{bbp}) are extracted using the criterion in Eq. (3). An example of the identified segments is shown in Figure 22. It should be emphasised that the shape of the reconstructed displacements is strongly dependent on these identified in-between bogie passages regions ("at rest positions"), and this method allows for automatic identification of these segments.

$$s_{\mathrm{a}}(t) = \int_0^t [a_{\mathrm{d}}(\tau)]^2 f_{2\mathrm{m}}(t-\tau)d\tau, \quad t \in [0,T] \qquad \text{Eq. 1}$$

$$f_{2\mathrm{m}}(t) = \begin{cases} 1/M, & t \in [-M/2, M/2] \\ 0, & \text{otherwise} \end{cases} \qquad \text{Eq. 2}$$

$$s_{\mathrm{bbp}}(t) = \begin{cases} 1, & s_{\mathrm{a}}(t)/\max\left(s_{\mathrm{a}}(t)\right) < 0.02 \\ 0, & \text{otherwise} \end{cases} \qquad \text{Eq. 3}$$

Step 2. After detrending, the signal is zero-padded according to Eq. (4). The zero-padding to the power of 2^n optimises the computation of the Discrete Fourier Transform (DFT) with the Fast Fourier Transform (FFT). With n equal to 19 ($N = 2^{19}$) and sampling frequency $f_{\mathrm{s}} = 20$ kHz, the achieved resolution in the frequency domain is about 0.04 Hz. This step allows for smoother high-pass filtering at low frequencies compared to what would have been achieved by a DFT with a frequency resolution of about 0.2 Hz corresponding to a typical train passage duration of 5 s.

$$a_{\mathrm{dz}}(t) = \begin{cases} a_{\mathrm{d}}(t), & t \in [0,T] \\ 0, & t \in (T, N/f_{\mathrm{samp}}] \end{cases} \qquad \text{Eq. 4}$$

Step 3. The Frequency Domain Integration (FDI) is performed. The zero-padded signal $a_{\mathrm{dz}}(t)$ is discretised to $a_{\mathrm{dz}}[n]$ with n limits $[-N/2, N/2-1]$ formed for obtaining a symmetric DFT. Next, $a_{\mathrm{dz}}[n]$ is transferred to the frequency domain via a DFT, see Eq. (5). In Eq. (6), an angular frequency domain is defined and used in Eq. (7) to obtain a transfer function $H[k]$ for the double integration in the frequency domain. Further, the frequency-domain acceleration signal $A_{\mathrm{dz}}[k]$ is element-wise multiplied with the digital integrator $H[k]$ and subjected to the frequency-domain high-pass filter at a frequency f_p where the parameter p is the corresponding sample number, see Eq. (8). The high-pass filter frequency is optimised in Step 5. Next, this signal is transformed back to the time domain with the IDFT, see Eq. (9). The result of Step 3 is displacements $d_{\mathrm{int}}[p,n]$ that are dependent on the parameter p. The obtained displacements $d_{\mathrm{int}}[p,n]$ are of length T with zero phase shift relative to the initial acceleration signal.

$$A_{dz}[k] = \sum_{n=-N/2}^{N/2-1} a_{\mathrm{dz}}[n] e^{-\frac{i2\pi k}{N}n}, \quad -N/2 \le k \le N/2-1 \qquad \text{Eq. 5}$$

$$\omega[k] = \frac{2\pi f_{\mathrm{s}}}{N} k \ , \qquad N/2 \le k \le N/2-1 \qquad \text{Eq. 6}$$

$$H[k] = \begin{cases} -1/(\omega[k])^2, & N/2 \le k \le N/2-1 \\ 0, & k = 0, \end{cases} \qquad \text{Eq. 7}$$

$$D[p,k] = \begin{cases} A_{dz}[k]H[k], & -N/2 \le k < -p, \\ 0, & -p \le k \le p, \\ A_{dz}[k]H[k], & p < k \le N/2-1, \end{cases} \qquad 0 < p \le N\frac{f_0}{f_{\mathrm{s}}} \ , \qquad \text{Eq. 8}$$

$$f_p = \frac{f_{\mathrm{s}}}{N} p$$

$$d_{\mathrm{int}}[p,n] = \frac{1}{N} \sum_{k=-\mathrm{N}/2}^{\mathrm{N}/2-1} D[p,k] e^{\frac{i2\pi k}{N}n}, \qquad \text{Eq. 9}$$

$$-f_{\mathrm{s}}T/2 \le n \le f_{\mathrm{s}}T/2-1, \quad 0 < p \le N\frac{f_0}{f_{\mathrm{s}}}$$

Step 4. The integrated displacements d_{int} are detrended to the "at rest position". This is achieved by a linear fit b_{f} to the displacement curve d_{int} at the identified locations s_{bbp} between bogie passage locations from Eq. (3). The obtained curve b_{f} is smoothened with a 10-metre wavelength low-pass filter. The obtained filtered curve b_{f10m} is used as a baseline detrend. It is subtracted from d_{int} to obtain the baseline detrended displacements d_{bd}, see Eq. (10) and Figure 22.

$$d_{\mathrm{bd}}[p,n] = d_{\mathrm{int}}[p,n] - b_{\mathrm{f10m}}[p,n],$$
$$n = [-f_{\mathrm{s}}T/2, f_{\mathrm{s}}T/2-1], \quad 0 < p \le N\frac{f_0}{f_{\mathrm{s}}} \qquad \text{Eq. 10}$$

Step 5. The final step of the displacement reconstruction is to find the optimum value *p* for the high-pass filter frequency f_p. As the value of *p* increases, shorter time windows of displacements d_{bd} obtain zero mean due to the high-pass filtering. This means that above a certain *p,* the displacement signatures of individual bogie passages will become distorted. This will be observed as curve oscillations around the detrended baseline at the beginning and end of each bogie passage, which means that the magnitude of negative (upwards) displacements will start to increase. In the optimisation of *p,* a penalty is set for these negative displacements. The objective function in the optimisation also accounts for the standard deviation of d_{bd}. The standard deviation will start to increase if the d_{bd} baseline detrend residuals become higher due to low-frequency noise, or if d_{bd} encounters local distortions or global inclinations. Finally, the objective function is computed as a multiplication of these two functions and the product is minimised in the optimisation, see Eq. (11).

The optimisation is performed in two steps for frequencies between 0 and $f_0 = 2$ Hz. The first step is an exploration of the domain with a step length of 0.2 Hz for f_p. The second step is a fine optimisation with a step length of 0.04 Hz in the localised domain obtained from the initial exploration. Examples of reconstructions in the optimisation domain obtained with this exploration are presented in Figure 23. It shows various curves d_{int} with different baselines. Each of the bogie passage segments will be affected differently by the baseline detrend after subtracting $b_{\mathrm{f10m}}[p, m]$.

With the presented optimisation scheme, a stable displacement reconstruction is secured. The complete displacement reconstruction method is developed to allow for large sets of data and long-term automatic processing of accelerations from the field with variable operational conditions and varying quality of measured data. An example of the result of the reconstructed displacement is presented in Figure 24.

$$p = \arg\min\left(\left(\sum_{n=0}^{M-1}(d_{\mathrm{bd}}[p,n] < 0)\right)\sigma_{\mathrm{bd}}\right), \qquad 0 < p \leq N\frac{f_0}{f_{\mathrm{samp}}} \qquad \text{Eq. 11}$$

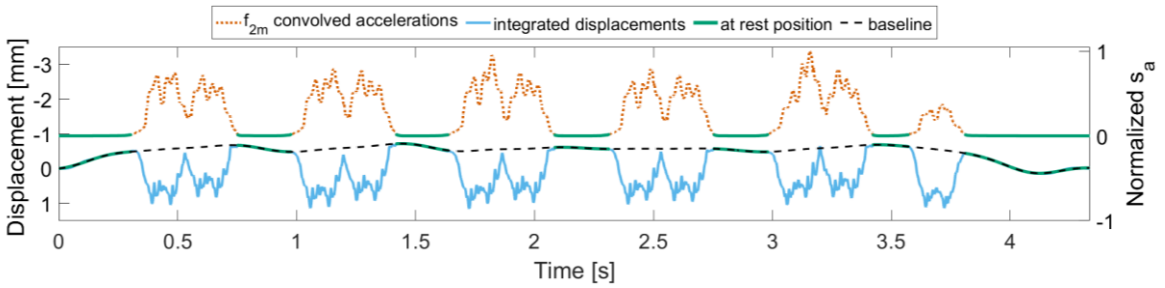

Figure 22 Integrated sleeper displacement before baseline detrending (scale on the left ordinate), and the product of convolution between acceleration signal and moving average filter, $\boldsymbol{s_a}$ Eq.(1) (scale on the right ordinate). The green segments are identified as regions between bogie passages.

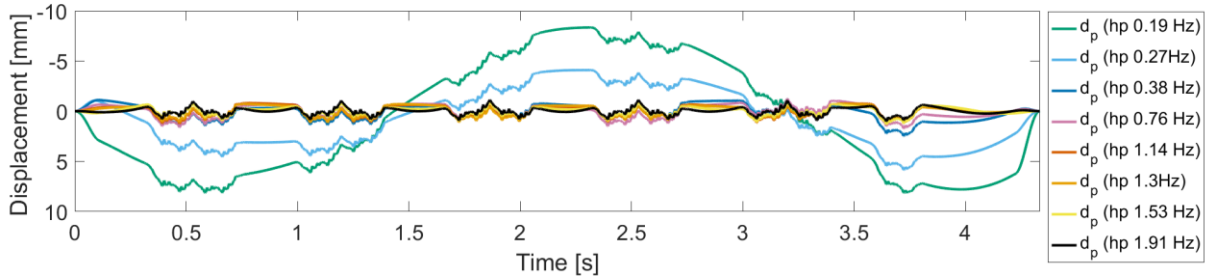

Figure 23 Integrated sleeper displacement for different high-pass frequencies $\boldsymbol{f_p}$ before in-between-bogie baseline detrending.

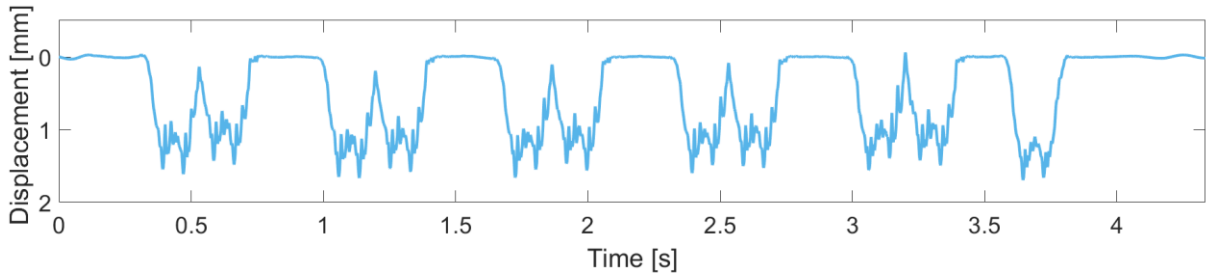

Figure 24 Example of final reconstructed displacement from the displacement reconstruction algorithm with the optimum $\boldsymbol{f_p} = 1.3$ Hz. Signal from X2 train with the first bogie passages discarded due to a signal-corrupting sensor wake-up transient.

5.6 Train speed identification

To obtain more detailed information about the traffic loading associated with the condition monitoring data, a train speed and train type identification method has been developed in **Paper B**. The method operates by cross-correlating new acceleration signals from passages of unknown trains with reference signals from known train passages. For the known train passages, the train type and speed have been manually identified by matching the axle locations of a given train type to the acceleration peaks in the signal. All signals are low-pass filtered at 20 Hz before the cross-correlation is computed. For this frequency range, it is observed that the sleeper displacement signature due to each axle passage has a close fit to the quasi-static loading displacement pattern and that similarities between different signals indicate the same train axle composition.

In the algorithm, each reference signal is first resampled to the train speed range from 20 to 60 m/s at intervals of 0.1 m/s. A small speed increment is used as the method is sensitive to train speed. The reference signals are named $a_{v-\mathrm{ref}}$ with length $T_{v-\mathrm{ref}}$, where v indicates the associated train speed. Each reference signal is normalised by its RMS value, and the new signal a_{lp20Hz} to be evaluated (with length T) is also RMS-normalised. Then the signals are cross-correlated according to Eq. (13) for all sampled train speeds from 20 to 60 m/s.

When an RMS-normalised signal is cross-correlated with itself, the maximum product is equal to 1. In this paper, if the satisfaction criterion in Eq. (14) (80% similarity) is fulfilled, the new acceleration recording is classified as the identified train type with the corresponding train speed from Eq. (14). An example of the function max $(c_v(t))$, where an X2 high-speed passenger train is identified, is shown in Figure 25(a). Another example, where the train passage is not identified by reference signals train types is presented in Figure 25(b). For each monitored crossing panel, a different set of reference acceleration signals needs to be created with classified train groups. To increase the accuracy of the method, multiple reference signals are stacked together (time-wise continuation), see Eq. (12).

$$a_{v-\mathrm{ref}}(t) = [a_{v-\mathrm{ref}\,1}(t), a_{v-\mathrm{ref}\,2}(t), \dots, a_{v-\mathrm{ref}\,\mathrm{n}}(t)], \quad v \in [20, 20.1, 20.2, \dots, 60]\ \mathrm{m/s} \qquad \text{Eq. 12}$$

$$c_v(t) = \int_{-T}^{T_{\mathrm{v-ref}}+T} a_{v-\mathrm{ref}}(\tau)\ a_{\mathrm{lp20Hz}}(t+\tau)\, d\tau,\ t = [0, T_{\mathrm{ref}} + T], \quad v \in [20, 20.1, 20.2, \dots, 60]\ \mathrm{m/s} \qquad \text{Eq. 13}$$

$$v_t = v \text{ for max } (c_v(t)) \text{ if } \max (c_v(t)) > 0.80, \qquad v \in [20, 20.1, 20.2, \dots, 60] \text{ m/s} \qquad \text{Eq. 14}$$

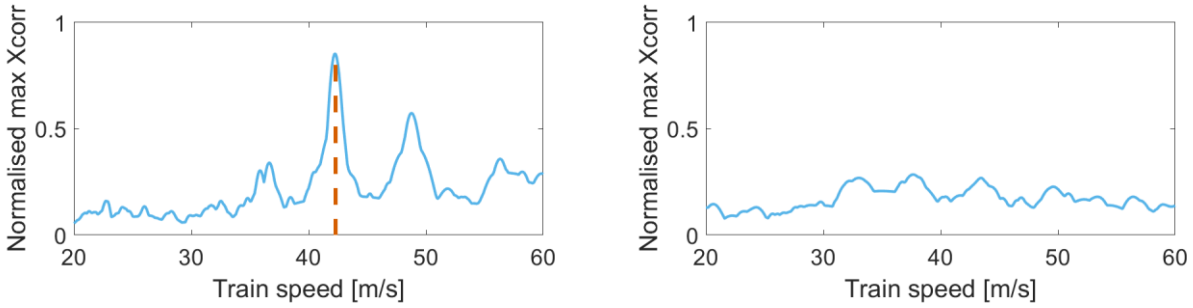

(a) **(b)**

Figure 25 Examples where the train passage is (a) identified or (b) not identified as an X2 high-speed passenger train. The continuous line presents max $c_v(t)$, while the dashed line presents the identified train speed, see Eq. (14).

Additionally,for verification of the method part of the data that was received from Trafikverket had information on train speed and type that was identified with the use of machine-learning classifiers.

5.7 Green's functions and inverse problem solving

In this section, the two GKFM concepts used in **Paper F** are presented. The first establishes a relation between the moving vertical force and the system response at a fixed node, while the second establishes a relation between the moving vertical force and the moving system response.

The Green's function is a unit impulse response function for the time-domain relationship between an input acting at the fixed location and the output system response at some also fixed location. In the following equations it is written as $g_{\mathrm{S}}^{\mathrm{r}m}(\mathrm{t})$, where r_m refers to the input location (r from rail) and S to the output system response (S from the sensor). The Green's function $g_{\mathrm{S}}^{\mathrm{r}m}(\mathrm{t})$ is calculated using the inverse Fourier transform of the receptance $h_{\mathrm{S}}^{\mathrm{r}m}$, which is computed from the FEM model. The equation is given in Eq. 15:

$$g_{\mathrm{S}}^{\mathrm{r}m}(t) = \mathcal{F}^{-1} h_{\mathrm{S}}^{\mathrm{r}m}(\omega) \qquad \text{Eq. 15}$$

For the crossing panel, by considering several fixed positions of the force acting along the crossing panel the track structure, the force and sensor nodes are illustrated in **Figure 26** . In this case, the FEM model is meshed such that it has 73 nodes along the straight route rails. In **Figure 27**, 73 Green's functions relating to the force at 73 rail nodes and the response at the sensor node are presented.

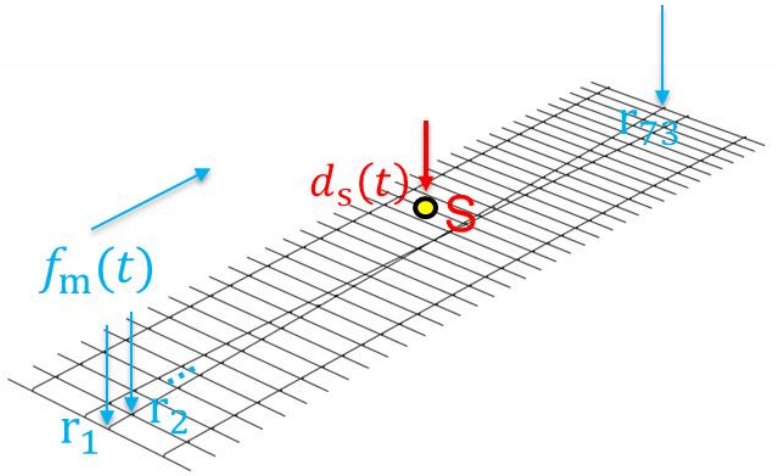

Figure 26 Single Green's function spatial input-output relation and used track structure model.

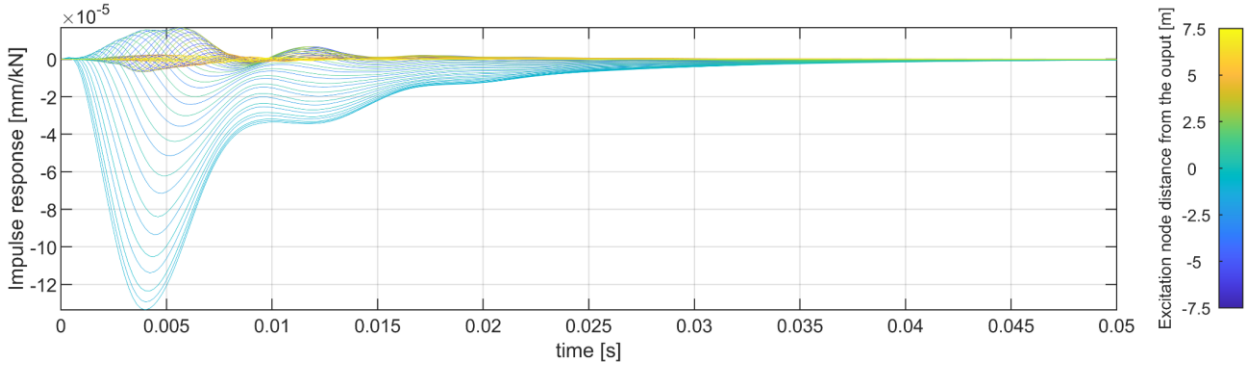

Figure 27 Example illustrating 73 Green's functions computed for the response at crossing sleeper node S due to impulse force acting at 73 FE rail nodes along a 15 m long track section (corresponding to 15 m bogie travel in the analysis).

5.7.1 Green's Kernel Function Method for Fixed Response (GKFM-FR)

In deriving the GKFM that links the displacement response of a sleeper and the force acting on the rail, an initial convolution integral needs to be introduced. For a single force acting at rail node m (r_m), the displacement response $d_S^{r_m}$ at the sensor S can be computed as Eq. 16 ([59]):

$$d_S^{r_m}(t) = \int_0^t g_S^{r_m}(\tau) f_{r_m}(t-\tau) d\tau = g_S^{r_m}(t) * f_{r_m}(t) \qquad \text{Eq. 16}$$

The discrete versions of $d_S^{r_m}(t), g_S^{r_m}(t)$ and $f_{r_m}(t)$ are denoted $d_S^{r_m}(n), g_S^{r_m}(n)$ and $f_{r_m}(n)$, respectively, while the corresponding time steps for a uniformly discretised time duration with N steps are obtained as $t = \Delta t(n-1)$. The convolution operation of Eq. 16 can be written in matrix format as shown in Eq. 17 [43]:

$$\begin{bmatrix} d_{\mathrm{S}}^{\mathrm{r}_m}(n_1) \\ d_{\mathrm{S}}^{\mathrm{r}_m}(n_2) \\ \vdots \\ d_{\mathrm{S}}^{\mathrm{r}_m}(n_N) \end{bmatrix} = \begin{bmatrix} g_{\mathrm{S}}^{\mathrm{r}_m}(n_1) & 0 & \cdots & 0 \\ g_{\mathrm{S}}^{\mathrm{r}_m}(n_2) & g_{\mathrm{S}}^{\mathrm{r}_m}(n_1) & \cdots & 0 \\ \vdots & \vdots & \ddots & \vdots \\ g_{\mathrm{S}}^{\mathrm{r}_m}(n_N) & g_{\mathrm{S}}^{\mathrm{r}_m}(n_{N-1}) & \cdots & g_{\mathrm{S}}^{\mathrm{r}_m}(n_1) \end{bmatrix} \begin{bmatrix} f_{\mathrm{r}_m}(n_1) \\ f_{\mathrm{r}_m}(n_2) \\ \vdots \\ f_{\mathrm{r}_m}(n_N) \end{bmatrix} \Delta t \qquad \text{Eq. 17a}$$

and on compact form

$$\boldsymbol{d}_{\mathrm{S}}^{r_m} = \boldsymbol{G}_{\mathrm{S}}^{r_m} \boldsymbol{f}_{\mathrm{r}_m} \Delta t \qquad \text{Eq. 17b}$$

where $\boldsymbol{G}_{\mathrm{S}}^{r_m}$ is the Green's kernel matrix (GKFM). In order to derive the Green's kernel matrix for a moving load, a superposition of Eq. 17 is made by summing the contributions to the response at $\boldsymbol{y}_{\mathrm{S}}$ from forces acting at all nodes r_m

$$\boldsymbol{d}_{\mathrm{S}} = \sum_{m=1}^{N} \boldsymbol{G}_{\mathrm{S}}^{\mathrm{r}_m} \boldsymbol{f}_{\mathrm{r}_m} \Delta t \qquad \text{Eq. 18}$$

Then a force-discretisation is introduced, where f_{r_m} is only non-zero at node *m* at timestep *m* when the force is positioned at node *m*. Thus, the load acts only once at each node and moves at speed $v = \frac{\Delta l}{\Delta t}$, where Δl is the distance between each equidistant node. This means that only column *m* of $\mathbf{G}_{\mathrm{S}}^{\mathrm{r_m}}$ times $f_{\mathrm{r_m}}(n_{\mathrm{m}})$ results from each summation term in Eq. 18, leading to Eq. 19

$$\begin{bmatrix} d_{\mathrm{S}}^{\mathrm{r},v}(n_1) \\ d_{\mathrm{S}}^{\mathrm{r},v}(n_2) \\ \vdots \\ d_{\mathrm{S}}^{\mathrm{r},v}(n_N) \end{bmatrix} = \begin{bmatrix} g_{\mathrm{S}}^{\mathrm{r}_1}(n_1) & 0 & \cdots & 0 \\ g_{\mathrm{S}}^{\mathrm{r}_1}(n_2) & g_{\mathrm{S}}^{\mathrm{r}_2}(n_1) & \cdots & 0 \\ \vdots & \vdots & \ddots & \vdots \\ g_{\mathrm{S}}^{\mathrm{r}_1}(n_N) & g_{\mathrm{S}}^{\mathrm{r}_2}(n_{N-1}) & \cdots & g_{\mathrm{S}}^{\mathrm{r_N}}(n_1) \end{bmatrix} \begin{bmatrix} f_{\mathrm{r}_1}(n_1) \\ f_{\mathrm{r}_2}(n_2) \\ \vdots \\ f_{\mathrm{r}_N}(n_N) \end{bmatrix} \Delta t \quad \text{where } \Delta t = \frac{\Delta l}{v} \qquad \text{Eq. 19}$$

For an input force moving along the rail at speed *v*, the matrix in Eq. 8 is the GKFM for a fixed response $\boldsymbol{G}_{\mathrm{S}}^{\mathrm{r,v}}$ (GKFM-FR) at node S. This equation presents the basis for inverse problem-solving and moving force identification.

As the FE model is meshed to have 73 nodes along the rail (30 cm equidistant spacing) on which the force moves, the computed single Green's functions from Figure 27 need to be spatially interpolated to obtain the needed resolution to fit a particular moving force speed. This resolution also depends on the time-domain sampling rate of Green's functions. In the performed analysis, the sampling rate of 5000 Hz ($\Delta t = \frac{1}{5000}$ [s]) is used, which for a moving force at speed *v* = 180 km/h gives a needed spatial resolution $\Delta l = 1$ cm.

5.7.2 Inverse problem – wheel–rail contact forces identification

While the relation between a moving load and the sensor has been established in (Eq. 19), a passing train has more than one wheel that influences the sleeper response. In **Paper F**, the inverse problem is therefore formulated for a four-wheel single-bogie passage as it is assumed that axles further away will

have a minor influence on the response based on the "nearsightedness" of the sensor as discussed above, see response attenuation from Figure 27 (0.03s at 50 m/s gives almost full response attenuation after 1.5m). Thus, the GKFM-FRs that relate four moving wheel–rail contact forces $f_{\mathrm{r,v}}$ along the rails (see **Figure 28** for force labels) with the displacement response $y_{\mathrm{S}}^{\mathrm{r},v}$ at sleeper node S (see Eq. 20) becomes a superposition of the contributions from all four wheels:

$$d_{\mathrm{S}}^{\mathrm{bogie},v}(n) = G_{\mathrm{S}}^{\mathrm{fr},v} f_{\mathrm{fr},v}(n) + G_{\mathrm{S}}^{\mathrm{fl},v} f_{\mathrm{fl},v}(n) + G_{\mathrm{S}}^{\mathrm{rr},v} f_{\mathrm{rr},v}(n) + G_{\mathrm{S}}^{\mathrm{rl},v} f_{\mathrm{rl},v}(n) \qquad \text{Eq. 20}$$

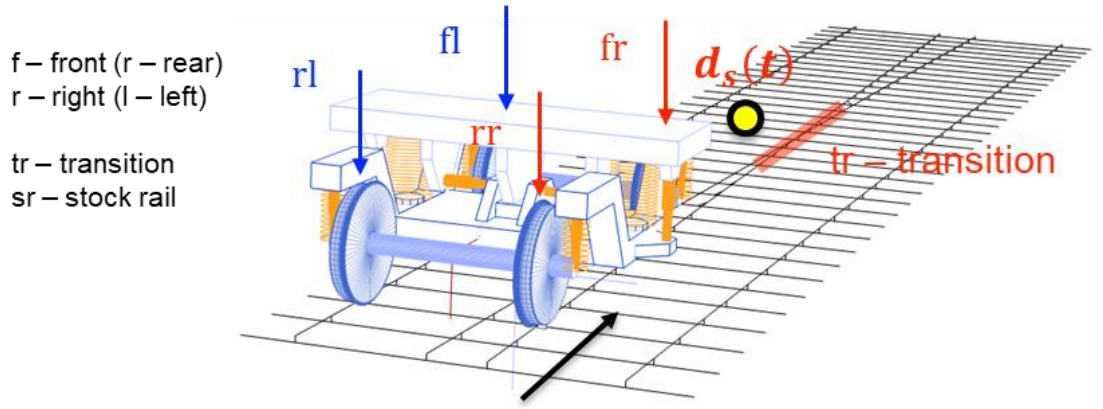

Figure 28 Bogie vehicle and track models with nomenclature for wheels, and sensor location marked with yellow dot. Marked transparent red region shows the section in which the wheel–rail contact forces are identified.

Further, the idea is to formulate the inverse problem related only to the isolated sleeper displacement response $d_{\mathrm{S}}^{\mathrm{bogie},v}$ in the sequence interval n_{tr1} to n_{tr2}, which is the displacement response for the time interval when the front right wheel is passing through the marked transition region TR in **Figure 28**, see Eq. 21. Generally, as the scalar product of one row in the GKFM and one column in the force vector sums up to one sequence of $d_{\mathrm{S}}^{\mathrm{bogie},v}$, the rows of GKFM are truncated while the force vectors are unaltered. This implies that a force positioned outside of the transition region influences the response $\left[\boldsymbol{d}_{\mathrm{S}}^{\mathrm{bogie},v}\right]_{n_{\mathrm{tr1}}:n_{\mathrm{tr2}}}$ as

$$\left[\boldsymbol{d}_{\mathrm{S}}^{\mathrm{bogie},v}\right]_{n_{\mathrm{tr1}}:n_{\mathrm{tr2}}} = \left[\boldsymbol{G}_{\mathrm{S}}^{\mathrm{fr},v}\right]_{n_{\mathrm{tr1}}:n_{\mathrm{tr2}},1:N}\left[\boldsymbol{f}_{\mathrm{fr},v}\right]_{1:N} + \left[\boldsymbol{G}_{\mathrm{S}}^{\mathrm{fl},v}\right]_{n_{\mathrm{tr1}}:n_{\mathrm{tr2}},1:N}\left[\boldsymbol{f}_{\mathrm{fl},v}\right]_{1:N} +$$
$$\left[\boldsymbol{G}_{\mathrm{S}}^{\mathrm{rr},v}\right]_{n_{\mathrm{tr1}}:n_{\mathrm{tr2}},1:N}\left[\boldsymbol{f}_{\mathrm{rr},v}\right]_{1:N} + \left[\boldsymbol{G}_{\mathrm{S}}^{\mathrm{rl},v}\right]_{n_{\mathrm{tr1}}:n_{\mathrm{tr2}},1:N}\left[\boldsymbol{f}_{\mathrm{rl},v}\right]_{1:N} \qquad \text{Eq. 21}$$

Next, by trivial separation of parts of the right front wheel and right rear wheel forces, the domain n_{tr1} to n_{tr2} is isolated, see Eq. 22. This formulation is taking into account an assumption that the rear wheel force is equal to the front wheel force shifted in time corresponding to the length of the bogie

axle spacing n_{bogie} $\left(f_{\mathrm{fr},v}(n) = f_{\mathrm{rr},v}\left(n + n_{\mathrm{bogie}}\right)\right)$. This enables the front wheel force expression $\left[\boldsymbol{f}_{\mathrm{fr},v}\right]_{n_{\mathrm{tr1}}:n_{\mathrm{tr2}}}$ to represent both forces acting in the crossing.

$$\left[\boldsymbol{f}_{\mathrm{fr},v}\right]_n = \begin{bmatrix} \left[\boldsymbol{f}_{\mathrm{fr},v}\right]_{1:n_{\mathrm{tr1}}} \\ \left[\boldsymbol{f}_{\mathrm{fr},v}\right]_{n_{\mathrm{tr1}}:n_{\mathrm{tr2}}} \\ \left[\boldsymbol{f}_{\mathrm{fr},v}\right]_{n_{\mathrm{tr2}}:N} \end{bmatrix}, \qquad \left[\boldsymbol{f}_{\mathrm{rr},v}\right]_n = \begin{bmatrix} \left[\boldsymbol{f}_{\mathrm{rr},v}\right]_{1:n_{\mathrm{tr1}}+n_{\mathrm{bogie}}} \\ \left[\boldsymbol{f}_{\mathrm{fr},v}\right]_{n_{\mathrm{tr1}}:n_{\mathrm{tr2}}} \\ \left[\boldsymbol{f}_{\mathrm{rr},v}\right]_{n_{\mathrm{tr2}}+n_{\mathrm{bogie}}:N} \end{bmatrix} \qquad \text{Eq. 22}$$

By combining the expressions for the isolated sequence interval n_{tr1} to n_{tr2} from Eq. 21, and decomposing the forces as in Eq. 22, the inverse problem for identifying the contact force in the transition region, $\left[\boldsymbol{f}_{\mathrm{fr},v}\right]_{n_{\mathrm{tr1}}:n_{\mathrm{tr2}}}$, is derived and presented in Eq. 23.

An additional prerequisite for solving Eq. 23 is that forces outside of the transition region are assumed to be known and equal to the quasi-static force due to the axle load of the identified train type. This means that all forces from the right-hand side of Eq. 23 are assumed to be known and equal to half of the axle load.

The formed matrix $\left(\boldsymbol{G}_{\mathrm{S}}^{\mathrm{fr},v} + \boldsymbol{G}_{\mathrm{S}}^{\mathrm{rr},v}\right)$ is an ill-conditioned, square matrix. Here, the inversion of this matrix is carried out by a Moore-Penrose left pseudo-inverse operation (†) [60, 61], which is based on singular value decomposition. For numerical computation, the tolerances related to the singular values of this pseudo-inversion operation are optimised by minimising the difference between the input displacements and the displacements computed with Green's functions and inversely identified forces.

$$\begin{aligned} \left[\boldsymbol{f}_{\mathrm{fr},v}\right]_{n_{\mathrm{tr1}}:n_{\mathrm{tr2}}} = & \left(\left[\boldsymbol{G}_{\mathrm{S}}^{\mathrm{fr},v}\right]_{n_{\mathrm{tr1}}:n_{\mathrm{tr2}},n_{\mathrm{tr1}}:n_{\mathrm{tr2}}} + \left[\boldsymbol{G}_{\mathrm{S}}^{\mathrm{rr},v}\right]_{n_{\mathrm{tr1}}:n_{\mathrm{tr2}},n_{\mathrm{tr1}}+n_{\mathrm{bogie}}:n_{\mathrm{tr2}}+n_{\mathrm{bogie}}}\right)^{\dagger} \cdot \\ & \cdot \Big(\left[\boldsymbol{y}_{\mathrm{S}}^{\mathrm{fr,fl,rr,rl},v}\right]_{n_{\mathrm{tr1}}:n_{\mathrm{tr2}}} - \left[\boldsymbol{G}_{\mathrm{S}}^{\mathrm{fl},v}\right]_{n_{\mathrm{tr1}}:n_{\mathrm{tr2}},1:N} \left[\boldsymbol{f}_{\mathrm{fl,v}}\right]_{1:N} \\ & - \left[\boldsymbol{G}_{\mathrm{S}}^{\mathrm{rl},v}\right]_{n_{\mathrm{tr1}}:n_{\mathrm{tr2}},1:N} \left[\boldsymbol{f}_{\mathrm{rl},v}\right]_{1:N} - \left[\boldsymbol{G}_{\mathrm{S}}^{\mathrm{fr},v}\right]_{n_{\mathrm{tr1}}:n_{\mathrm{tr2}},1:n_{\mathrm{tr1}}} \left[\boldsymbol{f}_{\mathrm{fr},v}\right]_{1:n_{\mathrm{tr1}}} \\ & - \left[\boldsymbol{G}_{\mathrm{S}}^{\mathrm{fr},v}\right]_{n_{\mathrm{tr1}}:n_{\mathrm{tr2}},n_{\mathrm{tr2}}:N} \left[\boldsymbol{f}_{\mathrm{fr},v}\right]_{n_{\mathrm{tr2}}:N} \\ & - \left[\, \boldsymbol{G}_{\mathrm{S}}^{\mathrm{rr},v}\right]_{n_{\mathrm{tr1}}:n_{\mathrm{tr2}},1:n_{\mathrm{tr1}}+n_{\mathrm{bogie}}} \left[\boldsymbol{f}_{\mathrm{rr},v}\right]_{1:n_{\mathrm{tr1}}+n_{\mathrm{bogie}}} \\ & - \left[\, \boldsymbol{G}_{\mathrm{S}}^{\mathrm{rr},v}\right]_{n_{\mathrm{tr1}}:n_{\mathrm{tr2}},n_{\mathrm{tr2}}+n_{\mathrm{bogie}}:N} \left[\boldsymbol{f}_{\mathrm{rr},v}\right]_{n_{\mathrm{tr2}}+n_{\mathrm{bogie}}:N} \Big) \end{aligned} \qquad \text{Eq. 23}$$

In conclusion, the inverse problem formulation for the wheel–rail contact force identification at the transition relies on three assumptions: (I) the time histories of the front and rear wheel–rail contact forces on the crossing rail side are the same but just shifted in time (the time shift corresponding to bogie axle distance); (II) the front and rear wheel–rail contact forces on the stock rail side are constant and equal to half of the known quasi-static axle load; and (III) the front and rear wheel–rail contact forces on the crossing rail side outside of the transition region are constant and equal to half of the known quasi-static axle load, see **Figure 28** for the illustration of the crossing transition. This formulation of the inverse problem transforms the ill-posed problem of identifying four unknown wheel–rail contact forces from one output response to a problem of identifying one force from one output response, thus enabling stable inverse problem-solving with a unique solution.

5.7.3 Green's Functions Kernel Matrix for Moving Response (GKFM-MR)

In this section, the Green's function method is instead formulated for the relation between the response of a moving point due to a moving force using GKFM-MR. It is given in Eq. 24, and derived analogously to Eq. 8 via a superposition of impulse response contributions $g_{\mathrm{r}_j}^{\mathrm{r}_i}$ between rail excitation node i and rail response node j. Thus, this formulation requires the impulse response functions to be computed between each rail excitation node to all rail nodes downstream from it where the rail response is to be obtained.

$$\begin{bmatrix} d_{\mathrm{r}_1}^{\mathrm{r},v}(n_1) \\ d_{\mathrm{r}_2}^{\mathrm{r},v}(n_2) \\ \vdots \\ d_{\mathrm{r}_N}^{\mathrm{r},v}(n_{\mathrm{N}}) \end{bmatrix} = \begin{bmatrix} g_{\mathrm{r}_1}^{\mathrm{r}_1}(n_1) & 0 & \cdots & 0 \\ g_{\mathrm{r}_2}^{\mathrm{r}_1}(n_2) & g_{\mathrm{r}_2}^{\mathrm{r}_2}(n_1) & \cdots & 0 \\ \vdots & \vdots & \ddots & \vdots \\ g_{\mathrm{r}_N}^{\mathrm{r}_1}(n_N) & g_{\mathrm{r}_N}^{\mathrm{r}_2}(n_{N-1}) & \cdots & g_{\mathrm{r}_N}^{\mathrm{r}_N}(n_1) \end{bmatrix} \begin{bmatrix} f_{\mathrm{r}_1}(n_1) \\ f_{\mathrm{r}_2}(n_2) \\ \vdots \\ f_{\mathrm{r}_N}(n_N) \end{bmatrix} \Delta t \qquad \text{Eq. 24}$$

The full expression for the moving rail displacement under the front right wheel–rail contact excited by the four wheel-rail contact forces of one bogie is presented in Eq. 25:

$$d_{\mathrm{fr},v}^{\mathrm{bogie},v}(n) = G_{\mathrm{fr},v}^{\mathrm{fr},v} f_{\mathrm{fr},v}(n) + G_{\mathrm{fr},v}^{\mathrm{fl},v} f_{\mathrm{fl},v}(n) + G_{\mathrm{fr},v}^{\mathrm{rr},v} f_{\mathrm{rr},v}(n) + G_{\mathrm{fr},v}^{\mathrm{rl},v} f_{\mathrm{rl},v}(n) \qquad \text{Eq. 25}$$

To calculate the rail displacements $d_{\mathrm{fr},v}^{\mathrm{bogie},v}$, the identified wheel–rail contact forces from the inverse problem-solving are used. These rail displacements together with the wheel displacements will be used to reconstruct the relative wheel–rail trajectories that will be presented in the next section.

5.8 Crossing irregularity identification

In this section, the formulation of the crossing irregularity reconstruction problem of **Paper F** is presented. For a perfectly round wheel making the crossing transition, the irregularity represents the vertical profile of the wheel movement with respect to the rail.

The steps for determining the irregularity are as follows:

1. Formulation of a Free Body Diagram (FBD) for the wheel, where the wheel load $Q_{\mathrm{axle}}/2$ and the inversely identified wheel–rail contact force $f_{\mathrm{fr},v}$ (front right wheel) are acting, see **Figure 29**. The wheel load is assumed to be constant and independent of the wheel displacement. This is reasonable since the relatively small wheel displacements would only result in minor changes in the spring suspension forces.
2. Calculation of the wheel acceleration based on the formulated FBD, see Eq. 26. Thus,

$$a_{\mathrm{w}}(t) = \frac{\frac{Q_{\mathrm{axle}}(t)}{2} - f_{\mathrm{fr},v}(t)}{\frac{m_{\mathrm{w}}}{2}} \qquad \text{Eq. 26}$$

3. Integration of the absolute wheel displacement from the calculated wheel acceleration.
4. Calculation of rail displacement beneath the wheel contact point using the identified wheel–rail contact forces and GKFM-MR, see Eq. 25.

5. Calculation of the relative difference between the displacement of the wheel and the rail. This is the crossing irregularity, see Eq. 27.

The wheel displacement calculation in Step 3 is a double integration performed in the frequency domain analogous to the method presented in [62]. The result from Step 5 is the wheel–rail relative vertical displacement that is governed by the discontinuity of the crossing in the transition from wing rail to the crossing nose. The equation for the calculation of the irregularity is presented in Eq. 27:

$$d_{\mathrm{wrt}} = \iint a_{\mathrm{w}}(t)dt - d_{\mathrm{fr}}^{\mathrm{bogie},v}(t) \qquad \text{Eq. 27}$$

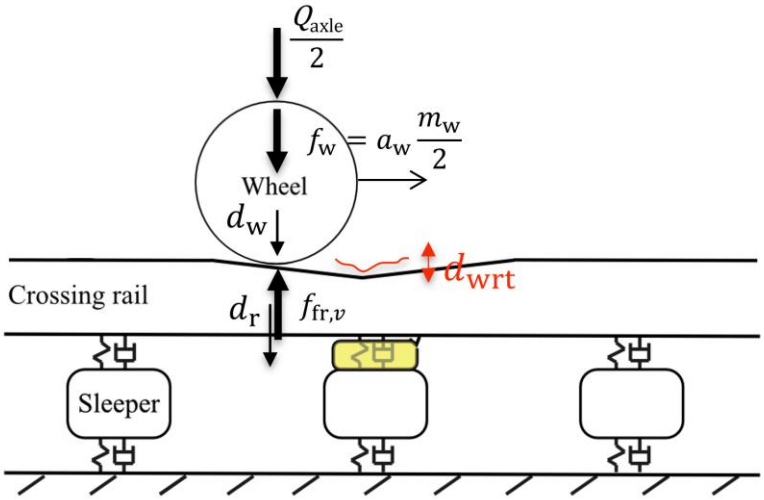

Figure 29 Free Body Diagram with the (1) half axle load, (2) mass and acceleration of the wheelset, and (3) inversely identified wheel–rail contact force

6 Summary of appended papers

Paper A: On tailored signal processing tools for operational condition monitoring of railway switches and crossings

This paper focuses on the development of tailored signal processing tools to analyse acceleration signals obtained from sensors placed on the sleeper beneath the railway crossing. The analysis is centred around examining the time-based and frequency-based properties of recorded accelerations, and how they are reconstructed into displacements.

In total, accelerations obtained from 41 train passages were analysed for two distinct crossing panels. Based on the analysed data, which are condensed as the root mean square of the processed accelerations and displacements, it is evident that there is a distinct difference in the responses of the two crossing panels.

The displacement reconstruction approach that is developed involves applying a low-pass filter to the acceleration signal followed by a two-step polynomial fit with high-pass filtering. The research demonstrates that the method produces accurate estimates of displacements that align well with direct measurements of track displacements. Further, the technique of Similarity Filtering is employed to selectively filter various parts of a signal, facilitating the straightforward extraction of dominant frequencies.

Paper B: Reconstruction of sleeper displacements from measured accelerations for model-based condition monitoring of railway crossing panels

This research focuses on the advancement of techniques for real-time monitoring of crossing panels by utilising operational acceleration measurements. The effort is directed at addressing a specific deficiency in the existing literature on S&C condition monitoring: the absence of a methodology that especially focuses on the signal processing component of S&C condition monitoring, and that places S&C operational condition monitoring evaluations into the context of the railway network while showcasing reliable and efficient processing of measurement data at a wide scale.

Recorded data from 100,000 train passages in eight crossing panels was used to do the acceleration measurement analysis. Using the provided data, a new approach for reconstructing displacement in the frequency domain is developed. The capacity of the developed method to handle significant variations in the measured data is shown, indicating its robustness. A train type and speed identification algorithm is constructed to accurately determine the specific train types and collect more detailed information about the operational loading of the assets. The provided condition monitoring method is fully automated, starting from loading the dataset of recorded accelerations and ending with the post-processed final results. A parameter investigation was conducted using multi-body simulations for the dynamic vehicle–track interaction in the crossing panel to assist in interpreting the processed data.

Paper C: Condition monitoring of railway crossing geometry via measured and simulated track responses

This paper presents developments for model-based condition monitoring of crossing panels. The study is built around concurrently scanned crossing rail geometries and measured sleeper accelerations from six crossing panels. The scanned geometries and a structural representation of the crossing panel are implemented in a multi-body simulation tool from which the wheel–rail contact forces and corresponding dynamic track response are analysed for a sample of measured wheel profiles. The main areas of investigation include wheel-crossing interaction kinematics, calibration of track models to measured track responses, and a proposed condition indicator for crossing geometry.

The results demonstrate a high level of agreement between the measured and simulated sleeper displacements, ranging from satisfactory to outstanding. The suggested indicator for the condition of the crossing geometry, which is based on the root mean square of a signal representing the dynamic response of a sleeper within a specified band-pass frequency range, exhibit a significant association with both the maximum wheel–rail contact force and the condition of the crossing rail geometry. The strong correlation between the measured and simulated track responses indicates that the indicator can be employed to qualitatively assess the condition of crossing geometry. Nevertheless, inconsistencies between the measured and simulated values indicate that the in-situ parameters can have a substantial impact on the results.

Paper D: Demonstration of a Digital Twin framework for model-based operational condition monitoring of crossing panels

This paper outlines the beginning phases of developing a Digital Twin framework for utilising models to monitor the condition of railway switches and crossings. The study uses scanned crossing rail geometry and recorded sleeper accelerations from two crossing panels. The primary research areas involve analysing long-term patterns, the influence of environmental conditions on monitoring data, and the calibration of track models with measured track responses. The calibration of models relies on recorded data of sleeper displacements, velocities, and accelerations. The results demonstrate a high level of agreement between the measured and simulated responses, suggesting that the model calibration approach is suitable for identifying crossing panel conditions.

Paper E: Model-based remote health monitoring of ballast conditions in railway crossing panels

This paper introduces an automated calibration method for ballast parameters that has been validated using six in situ crossing panels. A brute force optimisation analysis is employed to compare two distinct ballast models. Additionally, a multiparameter sensitivity analysis is conducted, leading to the identification of three specific parameters for ballast parameter determination. These parameters include the uniform ballast stiffness in a region located outside of the crossing transition, the minimal or maximal ballast stiffness within the crossing transition region, and a parameter governing the distribution of ballast stiffness in the crossing transition region. The method is determined to be sufficiently robust for the identification of ballast parameters in a railway crossing panel.

Paper F: Inverse wheel–rail contact force and crossing irregularity identification from measured sleeper accelerations – A model-based Green's function approach

This paper introduces a Crossing Panel Condition Monitoring (CPCM) technique that based on measured sleeper accelerations uses the Green's Kernel Function Method (GKFM) to detect the ballast condition, vertical wheel–rail contact forces, and crossing geometry in a crossing panel. The method employs a multi-body simulation model using a finite element method (FEM) track model to establish a physics-informed link between input forces and output responses and an inverse load identification technique based on GKFM. The approach is developed using concurrently measured sleeper acceleration data and laser-scanned crossing geometries from six crossing panels.

The paper demonstrates the feasibility of determining ballast stiffness properties without prior knowledge of the crossing geometry, thus enabling the use of single location response-moving force GKFM for inverse wheel–rail contact force identification. Additionally, the study shows that relative wheel–rail trajectories in a particular wavelength range can be identified using a moving response-moving force GKFM and the previously identified wheel–rail contact forces.

A high level of agreement is seen between the quantities derived from the measured data and those obtained from the simulation environment. Additionally, the results indicate a higher level of variability among the responses observed in the field measurements, except for two hollow-worn wheel profiles whose simulation results deviate significantly from more regular wheel profiles. However, it is concluded that there is a notable and consistent qualitative correlation between the measurements and simulations.

7 Discussion

This research project interacts with the fields of data acquisition, signal processing, structural mechanics, multi-body dynamics, geotechnics, material science, and data analytics. Considering that the developed Digital Twin system is to operate in a non-research environment, each field brings some assumptions, simplifications, and limitations to reach an optimal level of results accuracy with a feasible computational effort.

The overall framework starts with the acquisition of a change in electrical current in the sensor due to vibrations and its transformation to acceleration. This process can be affected by the temperature of sensor parts [63] and environmental conditions, as well as by some level of long-term deterioration of the sensor itself. Together they negatively contribute to the sensor's digital noise and performance. An additional difficult challenge related to the temperature effects is to understand and distinguish its influence on the structural response from the sensor response itself (the sensors transfer function). For example, solar radiation as a source of temperature load can cause a temperature difference between the air and rail of up to 40°C [64]. This can cause an increase in rail stress and possibly rail expansion and track deformation. On the other hand, cold weather can induce cracks due to tension [65]. The overall significance of the possible temperature effect depends on the track structural design that in different ways can govern the thermal expansion. Studying the influence of environmental conditions on crossing panel dynamic response [66] established a correlation between the measured acceleration responses and the environmental conditions. Findings are verified with the MBS model which incorporates the environmental conditions by applying deformation from thermal load. The study concluded a relation between dynamic response fluctuations and environmental conditions, particularly the effect of solar radiation. In **Paper D**, long-term temperature effects are studied and their influence is detrended, but a separation of effects on the sensor and the structure is not conducted. Such an investigation can be found in [67] for general influence of temperature on sensors.

Further, as data comes from a remote continuous monitoring system, the uncertainties in the recorded train passages are unknown, and output variability is observed to be at a high level. This is addressed by identification of train type and speed with a white-box cross-correlation algorithm. Based on grouping by train type and speed, this reduces the variability of recorded output. For passenger trains, axle loads are estimated from train type information (not accounting for passenger load). However, for freight trains, this information remains completely unknown making freight vehicle passage recordings much more difficult to process. Concerning the structural mechanics and geotechnics aspects of the project, the ballast is modelled as a discrete, linear or bilinear (accounting for sleeper voids), system, while the rails, sleepers and fasteners are represented by a linear system that is subjected to model size reduction by application of finite element condensation. Lastly, the vehicle used in the project represents a standardised train vehicle with rigid wheels, and it is reduced to a single bogie.

Most of the specified parameters, from material to vehicle suspension parameters are taken from other research, mostly from other CHARMEC projects [6-8]. Using the initial MBS model, the simulation time for 15 m of bogie travel distance through a crossing panel was around 50 minutes. After a reduction of resolution of the mesh of the track model, the simulation time was decreased to 5 – 7 minutes, which is a more feasible computation time for the execution of thousands of simulations.

Data used in the project is of two types, recordings from remote sleeper accelerometers (one per asset) and 3D scans of crossing rails that are incorporated into MBS model. The 3D scans were performed on the crossing running surface covering wing rail and crossing nose with a total length

spanning from 1.7 to 2.7 m. A longer scan with possibly an additional scan of the stock rail on the outer track side could have enhanced the MBS simulations.

Further benefits to the project could have been achieved (1) on the data acquisition side by performing additional field measurements with multiple high-quality accelerometers installed on both sleepers and rails, using axle counters (for speed identification), direct sleeper displacement measurements, ultrasound scans of the crossing rails, and cameras to identify passing train types; and (2) on the asset management side by analysing more maintenance data concerning ballast tamping, rail grinding and welding, rail replacement, and their signatures on the crossing dynamic response.

Based on the data available in the project, methods have been developed and validated. Some limitations are clear and open the opportunity for future work. The value of the developed methods comes from the large size of the acquired data, which includes years of remote monitoring from multiple assets of different types. The performed work and the methods developed in the project have continuously attracted attention from the research community and industry with some cases of direct utilisation and application of the published research. In conclusion, the biggest identified limitations was the lack of insight into the sensor technology itself, and restricted opportunities for in-field and in-depth investigations of a particular outlier behaviour. Concerning the MBS model, it is concluded that the used models showed outstanding performance for the application and the range of behaviour that the models were designed to capture.

8 Conclusions and contributions of the thesis

The main result of this thesis is the development of a robust model-based condition monitoring framework for railway crossing panels that based on data from remote acceleration sensors can be used to determine sleeper support conditions and rail irregularity in the crossing panel. The key developments that constitute this framework are:

- A novel technique for reconstructing displacements from measured accelerations
- Demonstration of the separation of dynamics response into two domains governed by the conditions of the ballast support and the irregularity of the rail surface
- Condition monitoring indicators based on processed measured acceleration data
- Signal processing tools for automatised processing of large datasets of sleeper accelerations
- Routines for calibration of MBS models that incorporate crossing rail scans, remote acceleration measurements, and sleeper voids
- Automatised routines for calibration of ballast parameters in the MBS model based on remote acceleration data with no crossing rail geometry information
- Based on the Green's Kernal Function Method and using remote acceleration data, inverse problem solving for identification of wheel–rail contact force at a crossing transition
- Based on the Green's Kernal Function Method and inversely identified wheel–rail contact forces, forward problem solving for the reconstruction of relative wheel–rail trajectory in the crossing transition

In conclusion, this thesis shows that the condition of a crossing panel can be derived based on the acceleration response of a single sleeper. The observed variabilities in the measured dynamic responses between different train passages and different assets indicate that the condition of the crossing panel needs to be determined from its operational behaviour during vehicle–track interaction, and that the condition of the crossing panel needs to be derived from long-term data. This supports the embedded remote sleeper accelerometer solution and the concept of condition monitoring of crossing panels, in contrast to periodic visual inspections by track engineers that do not provide information on crossing panel operational behaviour or the use of inspection vehicles that do not provide the excitation variability that is encountered in operational traffic.

Based on the methods developed in this thesis, it is concluded that crossing irregularity has a strong correlation with the wheel–rail impact force, which governs the level of stress that the rail experiences and can be directly related to the rail deterioration rate. Concerning ballast parameters and sleeper support conditions, which is the second damage mode in the crossing panel that has been investigated in this thesis, it is concluded that measured sleeper accelerations can be robustly reconstructed into sleeper displacements and used for ballast condition identification. This overall completes the developed condition monitoring framework, which in a robust and automatised manner derives railway ballast condition, wheel–rail impact forces, and crossing rail geometrical irregularities for a crossing panel based on remote sleeper acceleration measurements.

References

[1] R. Skrypnyk, U. Ossberger, B.A. Pålsson, M. Ekh, J.C.O. Nielsen, Long-term rail profile damage in a railway crossing: Field measurements and numerical simulations, Wear, 472-473 (2021).
[2] A. Cornish, Life-time monitoring of in service switches and crossings through field experimentation, PhD thesis, Imperial College London, 2014.
[3] W.-J. Zwanenburg, Modelling degradation processes of switches & crossings for maintenance & renewal planning on the Swiss railway network, PhD thesis, Swiss Federal Institute of Technology Lausanne, 2009.
[4] Railway Handbook, Energy consumption and CO 2 emissions focus on passenger rail services. International Energy Agency (IEA) and International Union of Railways (UIC), uic. org/IMG/pdf/handb ook_iea-uic_2017_web3. pdf. Accessed Nov, (2017).
[5] O. Piterina, A. Masharsky, Energy consumption of Rail Baltica Project: Regional aspects of environmental impact, Economics and Culture, 16 (2019) 148-160.
[6] B. Pålsson, Optimisation of railway switches and crossings, PhD thesis, Chalmers University of Technology, Sweden, 2014.
[7] X. Li, Wheel–rail impact loads and track settlement in railway crossings, PhD thesis, Chalmers University of Technology, Sweden, 2019..
[8] R. Skrypnyk, Long-term rail damage evolution in railway crossings, PhD thesis, Chalmers University of Technology, Sweden, 2020.
[9] E. Kassa, C. Andersson, J.C.O. Nielsen, Simulation of dynamic interaction between train and railway turnout, Vehicle System Dynamics, 44 (2006) 247-258.
[10] E.T. Selig, J.M. Waters, Track geotechnology and substructure management, Thomas Telford, 1994.
[11] H. Jenkins, J. Stephenson, G. Clayton, G. Morland, D. Lyon, The effect of track and vehicle parameters on wheel/rail vertical dynamic forces, Railway Engineering Journal, 3 (1974).
[12] K. Wang, W. Cao, L. Xu, X. Yang, Z. Su, X. Zhang, L. Chen, Diffuse ultrasonic wave-based structural health monitoring for railway turnouts, Ultrasonics, 101 (2020) 106031.
[13] M. Sysyn, U. Gerber, O. Nabochenko, D. Gruen, F. Kluge, Prediction of rail contact fatigue on crossings using image processing and machine learning methods, Urban Rail Transit, 5 (2019) 123-132.
[14] A. Chudzikiewicz, R. Bogacz, M. Kostrzewski, R. Konowrocki, Condition monitoring of railway track systems by using acceleration signals on wheelset axle-boxes, Transport, 33 (2018) 555–566.
[15] A.S.J. Suiker, The mechanical behaviour of ballasted railway tracks, PhD thesis, Delft University of Technology, The Netherlands, 2004.
[16] M. Sysyn, O. Nabochenko, V. Kovalchuk, Experimental investigation of the dynamic behavior of railway track with sleeper voids, Railway Engineering Science, 28 (2020) 290-304.
[17] T. Dahlberg, M. Ekh, J.C.O. Nielsen, State-of-the-art study on railway turnouts: Dynamics and damage, Chalmers University of Technology, Sweden, 2004.
[18] I. Grossoni, P. Hughes, Y. Bezin, A. Bevan, J. Jaiswal, Observed failures at railway turnouts: Failure analysis, possible causes and links to current and future research, Engineering Failure Analysis, 119 (2021) 104987.
[19] U. Oßberger, W. Kollment, S. Eck, Insights towards condition monitoring of fixed railway crossings, Procedia Structural Integrity, 2017, pp. 106-114.
[20] S.O. Erikstad, Merging physics, big data analytics and simulation for the next-generation digital twins, High-Performance Marine Vehicles, (2017) 141-151.
[21] X. Liu, V.L. Markine, H. Wang, I.Y. Shevtsov, Experimental tools for railway crossing condition monitoring (crossing condition monitoring tools), Measurement: Journal of the International Measurement Confederation, 129 (2018) 424-435.
[22] I.A. Khouy, P.-O. Larsson-Kråik, A. Nissen, J. Lundberg, U. Kumar, Geometrical degradation of railway turnouts: A case study from a Swedish heavy haul railroad, Proceedings of the Institution of Mechanical Engineers, Part F: Journal of Rail and Rapid Transit, 228 (2014) 611-619.
[23] B.A. Pålsson, J.C.O. Nielsen, Dynamic vehicle-track interaction in switches and crossings and the influence of rail pad stiffness - Field measurements and validation of a simulation model, Vehicle System Dynamics, 53 (2015) 734-755.
[24] M. Mishra, J. Odelius, A. Thaduri, A. Nissen, M. Rantatalo, Particle filter-based prognostic approach for railway track geometry, Mechanical Systems and Signal Processing, 96 (2017) 226-238.
[25] In2Rail, Deliverable 2.4, Embedded & integrated sensors: System design selection, 2018.
[26] C. Stenström, J. Lindqvist, F. Andersson, Condition based maintenance using MEMS accelerometers: For faster development of IoT in railways, Infra Sweden, 2030 (2017).

[27] B.A. Pålsson, H. Vilhelmson, U. Ossberger, M. Sehner, M.D.G. Milosevic, H. Loy, J.C.O. Nielsen, Dynamic vehicle–track interaction and loading in a railway crossing panel – Calibration of a structural track model to comprehensive field measurements, Vehicle System Dynamics, 1-27 (2024).
[28] K. Six, K. Sazgetdinov, N. Kumar, G. Müller, D. Velic, W. Daves, R. Skrypnyk, B.A. Pålsson, A whole system model framework to predict damage in turnouts, Vehicle System Dynamics, 61 (2023) 871-891.
[29] S. Bruni, I. Anastasopoulos, S. Alfi, A. Van Leuven, G. Gazetas, Effects of train impacts on urban turnouts: modelling and validation through measurements, Journal of Sound and Vibration, 324 (2009) 666-689.
[30] B.A. Pålsson, R. Ambur, M. Sebès, P. Wang, J.-Y. Shih, D. Fan, J. Xu, J. Chen, A comparison of track model formulations for simulation of dynamic vehicle–track interaction in switches and crossings, Vehicle System Dynamics, 61 (2023) 698-724.
[31] P. Antunes, H. Magalhães, J. Ambrósio, J. Pombo, J. Costa, A co-simulation approach to the wheel–rail contact with flexible railway track, Multibody System Dynamics, 45 (2019) 245-272.
[32] H. Alizadeh Otorabad, Y. Bezin, I. Grossoni, P. Jorge, Finite element analysis of a crossing panel under dynamic moving load – effect of support conditions and implications on foot fatigue, Proceedings of the Institution of Mechanical Engineers, Part F: Journal of Rail and Rapid Transit, 237 (2023) 563-575.
[33] N. Chaar, M. Berg, Simulation of vehicle–track interaction with flexible wheelsets, moving track models and field tests, Vehicle System Dynamics, 44 (2006) 921-931.
[34] E. Kassa, J.C.O. Nielsen, Dynamic train–turnout interaction in an extended frequency range using a detailed model of track dynamics, Journal of sound and vibration, 320 (2009) 893-914.
[35] L. Baeza, A. Roda, J.C.O. Nielsen, Railway vehicle/track interaction analysis using a modal substructuring approach, Journal of Sound and Vibration, 293 (2006) 112-124.
[36] L. Baeza, H. Ouyang, A railway track dynamics model based on modal substructuring and a cyclic boundary condition, Journal of Sound and Vibration, 330 (2011) 75-86.
[37] K. Knothe, S.L. Grassie, Modelling of railway track and vehicle/track interaction at high frequencies, Vehicle system dynamics, 22 (1993) 209-262.
[38] O. Avci, O. Abdeljaber, S. Kiranyaz, M. Hussein, M. Gabbouj, D.J. Inman, A review of vibration-based damage detection in civil structures: From traditional methods to Machine Learning and Deep Learning applications, Mechanical Systems and Signal Processing, 147 (2021).
[39] L. Wang, Y. Shao, Fault feature extraction of rotating machinery using a reweighted complete ensemble empirical mode decomposition with adaptive noise and demodulation analysis, Mechanical Systems and Signal Processing, 138 (2020).
[40] M. Basseville, M. Abdelghani, A. Benveniste, Subspace-based fault detection algorithms for vibration monitoring, Automatica, 36 (2000) 101-109.
[41] L. Mevel, M. Basseville, A. Benveniste, M. Goursat, M. Abdelghani, L. Hermans, On the application of a subspace-based fault detection method, Proceedings of the 17th International Modal Analysis Conference, 1999, pp. 35-41.
[42] M. Döhler, F. Hille, L. Mevel, W. Rücker, Structural health monitoring with statistical methods during progressive damage test of S101 Bridge, Engineering Structures, 69 (2014) 183-193.
[43] J. Liu, X. Sun, X. Han, C. Jiang, D. Yu, A novel computational inverse technique for load identification using the shape function method of moving least square fitting, Computers & Structures, 144 (2014) 127-137.
[44] L. Zhang, Y. Zhu, H. Zhang, X. Zhu, Identification of dynamic load on cantilever beam using Green's function method and regularization technique, 39th Chinese Control Conference (CCC), IEEE, 2020, pp. 2786-2791.
[45] Y. Sun, L. Luo, K. Chen, X. Qin, Q. Zhang, A time-domain method for load identification using moving weighted least square technique, Computers & Structures, 234 (2020) 106254.
[46] S. Wu, Y. Zheng, Y. Sun, Q. Fei, Identify the stochastic dynamic load on a complex uncertain structural system, Mechanical Systems and Signal Processing, 147 (2021) 107114.
[47] S. Wu, Y. Sun, Y. Li, Q. Fei, Stochastic dynamic load identification on an uncertain structure with correlated system parameters, Journal of Vibration and Acoustics, 141 (2019) 041013.
[48] HandySCAN 3D – BLACK Series, THE TRULY PORTABLE METROLOGY-GRADE 3D SCANNERS, Available from: https://www.creaform3d.com/en/portable-3d-scanner-handyscan-3d, Access date: 2021-05-10.
[49] D. Han, Comparison of commonly used image interpolation methods, Proceedings of the 2nd International Conference on Computer Science and Electronics Engineering, Atlantis Press, 2013, pp. 1556-1559.
[50] B.A. Pålsson, J.C.O. Nielsen, Wheel-rail interaction and damage in switches and crossings, Vehicle System Dynamics, 50 (2012) 43-58.
[51] B.A. Pålsson, J.C.O. Nielsen, Track gauge optimisation of railway switches using a genetic algorithm, Vehicle System Dynamics, 50 (2012) 365-387.

[52] B.A. Pålsson, A linear wheel–crossing interaction model, Proceedings of the Institution of Mechanical Engineers, Part F: Journal of Rail and Rapid Transit, 232 (2018) 2431-2443.
[53] D.J. Rixen, A dual Craig–Bampton method for dynamic substructuring, Journal of Computational and applied mathematics, 168 (2004) 383-391.
[54] In2Track, Deliverable 2.2, Enhanced S&C Whole System Analysis, Design and Virtual Validation (final), Chapter 3, (2019).
[55] N. Pillai, J.-Y. Shih, C. Roberts, Evaluation of numerical simulation approaches for simulating train–track interactions and predicting rail damage in railway switches and crossings (S&Cs), Infrastructures, 6 (2021) 63.
[56] S. Iwnicki, Manchester benchmarks for rail vehicle simulation, Vehicle System Dynamics, 30 (1998) 295-313.
[57] Y.P. Bezin, Björn A., Multibody simulation benchmark for dynamic vehicle-track interaction in switches and crossings: Modelling description and simulation tasks. v3, University of Huddersfield https://doi.org/10.34696/s60x-ay18, (2019).
[58] J.J. Kalker, A fast algorithm for the simplified theory of rolling contact, Vehicle System Dynamics, 11 (1982) 1-13.
[59] A. Pieringer, Time-domain modelling of high-frequency wheel/rail interaction, PhD thesis, Chalmers University of Technology, Sweden, 2011.
[60] R. Penrose, A generalized inverse for matrices, Mathematical proceedings of the Cambridge philosophical society, Cambridge University Press, 1955, pp. 406-413.
[61] S.L. Brunton, J.N. Kutz, Data-Driven Science and Engineering: Machine Learning, Dynamical Systems, and Control, Cambridge University Press, Cambridge, 2019.
[62] M.D.G. Milošević, B.A. Pålsson, A. Nissen, J.C.O. Nielsen, H. Johansson, Reconstruction of sleeper displacements from measured accelerations for model-based condition monitoring of railway crossing panels, Mechanical Systems and Signal Processing, 192 (2023) 110225.
[63] C. Nagel, F. Ante, M. Putnik, J. Classen, J. Mehner, Characterization of temperature gradients on MEMS acceleration sensors, Procedia Engineering, 168 (2016) 888-891.
[64] Instruction of procedures at extreme weather conditions RLN00165, Version 002; ProRail: Utrecht, The Netherlands,, in: ProRail (Ed.), 2003.
[65] L. Chapman, J. Thornes, Y. Huang, X. Cai, V. Sanderson, S. White, Modelling of rail surface temperatures: a preliminary study, Theoretical and Applied Climatology, 92 (2008) 121-131.
[66] X. Liu, V.L. Markine, Correlation analysis and verification of railway crossing condition monitoring, Sensors, 19 (2019) 4175.
[67] J.-H. Bartels, R. Xu, C. Kang, R. Herrmann, S. Marx, Experimental investigation on the transfer behavior and environmental influences of low-noise integrated electronic piezoelectric acceleration sensors, Metrology, 4 (2024) 46-65.